RESEARCH ARTICLE

Amyloid-beta-dependent phosphorylation of collapsin response mediator protein-2 dissociates kinesin in Alzheimer's disease

Sara H. Mokhtar[1], Min Joung Kim[1], Kylie A. Magee[1], Pei Mun Aui[1], Speros Thomas[1], Maha M. Bakhuraysah[1], Amani A. Alrehaili[1], Jae Young Lee[1], David L. Steer[2], Rachel Kenny[3], Catriona McLean[4], Michael F. Azari[3, 5], Antonis Birpanagos[6], Ewlina Lipiec[7], Philip Heraud[8], Bayden Wood[8], Steven Petratos[1, *]

1 Department of Neuroscience, Central Clinical School, Monash University, Prahran, Victoria, Australia
2 Department of Biochemistry and Molecular Biology, Monash University, Clayton, Victoria, Australia
3 Department of Anatomy & Developmental Biology, Monash University, Clayton, Victoria, Australia
4 Department of Anatomical Pathology, Alfred Hospital, Prahran, Victoria, Australia
5 School of Health and Biomedical Sciences, RMIT University, Bundoora, Victoria, Australia
6 Division of Animal and Human Physiology, Department of Biology, National and Kapodistrian University of Athens, Ilisia, Athens, Greece
7 The Henryk Niewodniczanski Institute of Nuclear Physics, Polish Academy of Sciences, Department of Applied Spectroscopy, Radzikowskiego, Krakow, Poland
8 Centre for Biospectroscopy and Department of Microbiology, Monash University, Clayton, Victoria, Australia

Funding: *This study was supported by King Abdul-Aziz University postgraduate scholarship (to SHM); the National Multiple Sclerosis Society (USA) Project Grant ID #RG43981/1 (to SP).*

Abstract

Alzheimer's disease (AD) is a neurodegenerative disorder characterized by accumulation of amyloid plaques and neurofibrillary tangles. Prior to the development of these characteristic pathological hallmarks of AD, anterograde axonal transport is impaired. However, the key proteins that initiate these intracellular impairments remain elusive. The collapsin response mediator protein-2 (CRMP-2) plays an integral role in kinesin-1-dependent axonal transport and there is evidence that phosphorylation of CRMP-2 releases kinesin-1. Here, we tested the hypothesis that amyloid-beta (Aβ)-dependent phosphorylation of CRMP-2 disrupts its association with the kinesin-1 (an anterograde axonal motor transport protein) in AD. We found that brain sections and lysates from AD patients demonstrated elevated phosphorylation of CRMP-2 at the T555 site. Additionally, in the transgenic Tg2576 mouse model of familial AD (FAD) that exhibits Aβ accumulation in the brain with age, we found substantial co-localization of pT555CRMP-2 and dystrophic neurites. In SH-SY5Y differentiated neuronal cultures, Aβ-dependent phosphorylation of CRMP-2 at the T555 site was also elevated and this reduced the CRMP-2 association with kinesin-1. The overexpression of an unphosphorylatable form of CRMP-2 in neurons promoted the re-establishment of CRMP-2-kinesin association and axon elongation. These data suggest that Aβ-dependent phosphorylation of CRMP-2 at the T555 site may directly impair anterograde axonal transport protein function, leading to neuronal defects.

Correspondence to:
Steven Petratos,
steven.petratos@monash.edu.

orcid:
0000-0003-1211-4577
(Steven Petratos)

doi: *10.4103/1673-5374.233451*

Accepted: *2018-03-30*

Key Words: *amyloid-beta protein; kinases; collapsin response mediator protein; microtubules; kinesin; tubulin*

Introduction

Alzheimer's disease (AD) is the most prevalent neurodegenerative condition causing more than 60% of all dementia cases. The histopathological hallmarks include the accumulation of fibrillary forms of the 4 kDa amyloid-beta (Aβ) polypeptide as plaques, along with intracellular neurofibrillary tangles (NFTs), synaptic and neuronal loss characteristics during cerebral atrophy. The aberrant processing of amyloid precursor protein (APP) by beta-site APP cleaving enzyme (BACE-1) then γ-secretase can generate toxic Aβ peptides, namely $A\beta_{1–40}$ and $A\beta_{1–42}$. These small molecular weight peptides are likely released at the synapse as soluble species that can oligomerize (Lazarov et al., 2002). Recently, extracellular oligomeric Aβ has been shown to selectively bind cellular prion protein (PrP^C), thereby leading to neurite dysfunction at the post-synaptic density mediated through a Fyn kinase-dependent mechanism (Um et al., 2012). Moreover, it has been suggested that extracellular oligomeric Aβ correlates with the inhibition of anterograde axonal transport (Vossel et al., 2010, 2015; Sherman et al., 2016).

The collapsin response mediator proteins (CRMPs) are members of the dihydropyrimidinase-related neuronal phosphoprotein family that consists five isoforms, CRMP-1, CRMP-2, CRMP-3, CRMP4, CRMP5 (Charrier et al., 2003). The most well characterized of these isoforms, CRMP-2, is localized to the cytoplasm and neurites of post-mitotic neurons (Wang and Strittmatter, 1996; Bretin et al., 2005). CRMP-2 is expressed in regions of the adult brain that display the greatest plasticity such as the hippocampus, olfactory bulb, and cerebellum (Wang and Strittmatter, 1996; Inagaki et al., 2001; Veyrac et al., 2005). CRMP-2 demonstrates functional specificity within the distal portions of neurites, in synapses, and in growth cones during development (Goshima et al., 1995). Specific physiological functions of CRMP-2 include: the regulation of cell surface receptor endocytosis (Nishimura et al., 2003); kinesin-dependent

axonal transport (Kimura et al., 2005); growth cone collapse (Goshima et al., 1995; Brown et al., 2004); polarity and differentiation of developing neurons and neurite outgrowth (Inagaki et al., 2001); and the regulation of microtubule dynamics (Fukata et al., 2002; Yoshimura et al., 2005). These key neurobiological functions have been associated with specific phosphorylation events near the C-terminus of CRMP-2 through a concert of kinases (Arimura et al., 2005; Uchida et al., 2005; Yoshimura et al., 2005), all of which have been reported to culminate in neurite retraction. In primary neurons and neuroblastoma cells, over-expression of CRMP-2 results in axon elongation (Fukata et al., 2002). However, the over-expression of truncated CRMP-2 (without the C-terminus tubulin binding domain) inhibits axon growth, suggesting that this region can govern axonal growth dynamics (Inagaki et al., 2001; Fukata et al., 2002).

Developmentally, kinesin light chain-1 (KLC-1) interacts with the C-terminal domain of CRMP-2, suggesting that CRMP-2 may be a key partner in the transport of growth-related molecular cargo to the plus ends of microtubules (Kawano et al., 2005a). It is important to note that this C-terminus kinesin-binding domain is highly phosphorylated (Kimura et al., 2005; Taghian et al., 2012) and can be cleaved under specific neurodegenerative conditions (Touma et al., 2007). Therefore, a tantalizing hypothesis is that if these phosphorylation and/or cleavage events are occurring during the pathogenesis of AD, then targeting these molecular events may point to novel therapeutics in the pursuit of limiting cognitive decline in patients exhibiting neurodegeneration.

Our novel findings indicate that Aβ can modulate the key microtubule-associated protein CRMP-2 through direct phosphorylation at the Threonine555 site, rendering this molecule incapable of associating with the anterograde transport protein, kinesin-1. This specific dissociation of CRMP-2 and kinesin-1 could be re-established in the presence of Aβ only if the SH-SY5Y neuroblastoma cells were transfected to overexpress a form of CRMP-2 that was incapable of phosphorylation at the Thr555 site. Moreover, we are the first to report that CRMP-2 phosphorylation potentiates the dissociation from kinesin in AD brain samples suggesting that an anterograde transport deficit exists in neurons during neurodegeneration.

Materials and Methods

Affinity purified anti-phospho-Thr555-CRMP-2 polyclonal antibody generation and validation

Through a commercial agreement, we developed a phospho-specific CRMP-2 antibody that only reacts with the Thr555 (ROCK II) site (Merck Millipore, Darmstadt, Germany) (Petratos et al., 2012). Validation of specificity was performed by ELISA, western blotting, and Mass Spectrometry (see **Additional Figure 1**). Each well of a 96-well plate was coated with 0.1, 1.0, 2.0, 4.0, 5.0 and 10.0 μg/mL Phospho-Thr555 CRMP-2 protein in 0.05 M carbonate buffer (pH 9.6) overnight at 4°C. The wells were then washed three times with PBS (pH 7.4) and non-specific binding sites were blocked using 10% FCS/PBS. Sera from immunized rabbits against the Phospho-Thr555 CRMP-2 peptide were diluted in 10% FCS/PBS (1:10,000) and added into the wells in triplicate. After 2 hour incubation at room temperature, the serum was removed and wells were washed three times with PBS (pH 7.4). Peroxidase-conjugated sheep anti-rabbit IgM/IgG antibody (Silenus Laboratory, Melbourne, Australia) was prepared in 10% FCS/PBS then added into the wells and incubated for 2 hours at room temperature. The loosely adherent antibodies were then washed off using PBS (× 3). Wells were then developed with 20 mg o-phenylene-diaminedihydrochloride (OPD; Sigma-Aldrich, St Louis, MO, USA) for 30 minutes. The peroxidase-OPD reaction was finally halted with 25 μL of 3 M HCl and the optical density of each well was measured at 490 nm using an EIA microplate reader (Bio-Rad, Hercules, CA, USA).

Human post-mortem brain tissue

Human CNS tissue was obtained from the Victorian Brain Bank Network (VBBN) (Mental Health Research Institute [MHRI], Melbourne, Australia) under the National Health and Medical Research Council guidelines and the Monash University Human Ethics committee approval number CF13/1646-2013000831. The following tissues were used in the current study: multiple sclerosis (MS), Alzheimer's disease (AD), Huntington's disease (HD), fronto-temporal dementia (FTD), non-neurological disease control brain tissue (control) (**Table 1**). Postmortem interval did not exceed 27 hours with an average interval of ~18 hours. All specimens were obtained from the frontal lobe inclusive of grey and white matter, frozen under liquid nitrogen and then stored in the Brain Biobank (MHRI) (–80°C until required). All frozen brain tissues were ground with a mortar and pestle on dry ice, then lyzed using RIPA buffer for western blotting analysis. Paired frozen tissue samples were processed by cryostat sectioning for immunohistochemistry (described below).

Immunohistochemistry

Paraffin-embedded sections

Female and male Tg2576 or wild-type mice (weighing between 24 and 32 g) were bred and maintained for either 6 or 12 months at the University of Melbourne Animal facility (Melbourne, Australia). Experiments were performed in accordance with the Australian code of practice for the care and use of animals for scientific purposes, approved by the University of Melbourne Animal Ethics Committee (AEC#06224). Fixed, paraffin-embedded wild-type (n = 6) and transgenic Tg2576 (n = 16) mouse brains were cut into 10 μm serial sections on a conventional microtome (LeicaBiosystems, Wetzlar, Germany). The sections were de-waxed and heat antigen retrieval was performed with 0.1 M citrate buffer (pH 6.0). They were then incubated with proteinase K (20 μg/mL) (Qiagen, Hilden, Germany) for an hour at 37°C, followed by three washes with PBS. The sections were post-fixed with 4% paraformaldehyde (PFA) for 30 minutes at room temperature. They were then blocked with 10% (v/v) FBS/0.3% (v/v) Triton X-100 in PBS overnight at 4°C. Sections were incubated with monoclo-

nal mouse anti-phospho-PHF-Tau pSer202/Thr205 (AT8) antibody (1:50, Thermo Scientific, Waltham, MA, USA) and polyclonal rabbit anti-phospho-Thr555 CRMP-2 antibody (pT555 CRMP-2; 1:200) diluted in blocking buffer overnight at 4°C.

Cryostat sections

Freshly dissected brain tissue blocks from MS (n = 8), AD (n = 8), HD (n = 4), FTD (n = 7) and NNDC (n = 12) were embedded in Optimal Cutting Temperature (OCT) compound then cut into 10 μm serial sections on a cryostat. Briefly, the sections were fixed with 4% PFA for 30 minutes at room temperature. They were then blocked with 10% (v/v) FBS/0.3% (v/v) Triton X-100 in PBS overnight at 4°C. Sections were incubated with the monoclonal anti-phospho-PHF-Tau (AT8) antibody (1:50) or, monoclonal anti-NF200 antibody (1:200) (Thermo Scientific, Waltham, MA, USA) and polyclonal anti-phospho-Thr555 CRMP-2 antibody (1:200) diluted in blocking buffer overnight at 4°C.

Subsequently, both paraffin-embedded and cryostat sections were incubated with Alexa-Fluor 488 goat anti-rabbit IgG (1:200, Invitrogen) and Alexa-Fluor 555 goat anti-mouse IgG (1:200, Invitrogen) in blocking buffer at room temperature for an hour. The sections were incubated with DAPI (1:2000) for 15 minutes at room temperature and cover-slipped using fluorescent mounting medium (Agilent, Santa Clara, CA, USA). Images were captured under an oil 20×, 40× and 60× objective lens on the C1 upright confocal microscope (Nikon, Tokyo, Japan). The 16-bit images were converted to TIFF files using ImageJ software (Bethesda, MD, USA) and they were formatted using Adobe Photoshop CS3 software (San Jose, CA, USA). The percentage of co-labeled pT555CRMP-2 and AT8-positive neurons was calculated from the total number of neurons that were NF200-positive throughout 10 fields of view per section at ×20 magnification per section (n = 3 sections > 50 μm apart, per brain specimen).

Preparation of Aβ for cell culture

$A\beta_{1–40}$, $A\beta_{1–42}$, $ScrA\beta_{1–40}$ and $ScrA\beta_{1–42}$ stock solutions (rPeptides Inc.) were dissolved in dimethyl sulfoxide (DMSO) at a concentration of 10 μg/mL, and stored as aliquots at –20°C. An aliquot of $A\beta_{1–40}$, $A\beta_{1–42}$, $ScrA\beta_{1–40}$ and $ScrA\beta_{1–42}$ was dissolved in anhydrous DMSO to 10 μM, which was then added to ice-cold DMEM/F12 medium with FCS to 0.5, 1.0 and 10 μM. Differentiated human neuroblastoma SH-SY5Y cells (A gift from Professor David H Small, Menzies Research Institute, University of Tasmania, Hobart, Australia) were incubated with these Aβ peptides over a 24-hour period.

Atomic force microscopy (AFM)

$A\beta_{1–42}$ peptides were dissolved in DMEM/F12 medium (Invitrogen) supplemented in heat inactivated fetal calf serum (FCS) as prepared for the treatment of differentiated human neuroblastoma SH-SY5Y cells (see below). The final concentration of $A\beta_{1–42}$ peptide in solution was at 1 μM incubated at 37°C for 36 hours prior to imaging of Aβ aggregation. Application of $A\beta_{1–42}$ solutions (40 μL were deposited onto gold-coated mica and incubated at 37°C for 10 minutes prior to AFM imaging as previously performed (Petratos et al., 2008). $A\beta_{1–42}$ aggregated samples were viewed using a Digital Instruments Nanoscope IV Multimode scanning probe microscope (Veeco Instruments, Plainview, NY, USA), NSC15 125 μm cantilevers in tapping mode (250–350 kHz) and analyzed through WSxM 5.0 software (Nanotec Electronica, Madrid, Spain).

Human neuroblastoma SH-SY5Y cell culture

Human neuroblastoma SH-SY5Y cells were seeded at a density of 100,000 cells per well in 24-well plates in DMEM/F12 medium (Invitrogen) supplemented with 10% heat-inactivated FBS (Invitrogen) and 1% v/v penicillin/streptomycin (Invitrogen). After 24 hours, the cells were differentiated into a neuronal phenotype using 10 μM retinoic acid (RA) (Sigma-Aldrich) over a 7-day period. On day 8, RA treatment was removed and the medium was replaced with medium containing $A\beta_{1–40}$ peptide, $A\beta_{1–40}$ scrambled peptide, $A\beta_{1–42}$ peptide or $A\beta_{1–42}$ scrambled peptide at concentrations of 0.5, 1 or 10 μM. The cells were treated with these peptides overnight before they were washed and lysed for protein collection. Alternatively, SH-SY5Y cells were differentiated on coverslips and incubated with $FluoA\beta_{1–40}$ (1 μM) overnight then incubated on ice with AlexaFluor-555-conjugated Cholera toxin B subunit (250 ng/mL, Invitrogen) for 15 minutes, rinsed with ice-cold PBS (containing Mg^{2+} and Ca^{2+}) and fixed in 4% PFA for 30 minutes at room temperature. The cells were washed three times with ice-cold PBS and mounted on Superfrost Plus slides (Thermo Scientific, Waltham, MA, USA) using fluorescent mounting medium (Agilent, Santa Clara, CA, USA). Images were captured under an oil 20 ×, 40× and 60× objective lens on the Nikon C1 upright confocal microscope.

CRMP-2 mutant constructs and transfection of human neuroblastoma SH-SY5Ycells

Human CRMP-2 with N-terminal FLAG tag cloned into pRK5 mammalian expression vector was obtained from Dr. Lisa Ooms (Department of Biochemistry and Molecular Biology, Monash University, Melbourne, Australia). Site directed mutagenesis was performed (Agilent, Santa Clara, CA, USA) to produce the following CRMP-2 mutants: T509A, T514A, S518A, S522A, and T555A using the following primers; T509A forward 5′-gtg tga agt gtc tgt ggc gcc caa gac agt cac-3′, T509A reverse 5′-gtg act gtc ttg ggc gcc aca gac act tca cac-3′, T514A forward, 5′-gcc caa gac agt cgc tcc agc ctc ctc-3′, T514A reverse 5′-gag gag gct gga gcg act gtc ttg ggc-3′, S518A forward 5'-cac tcc agc ctc cgc ggc caa gac gtc-3', S518A reverse 5′-gac gtc ttg gcc gcg gag gct gga gtg-3′, S522A forward 5′-ctc ggc caa gac ggc tcc tgc caa gca-3′, S522A reverse 5′-tgc ttg gca gga gcc gtc ttg gcc gag-3′, T555A forward 5′-ccc gcc gca ccg ccc agc gta tc-3′, T555A reverse 5′-gat acg ctg ggc ggt gcg gcg gg-3′. The CRMP-2 mutant constructs with FLAG tag were then subcloned into pCMV-Tag5 mammalian expression vector (Agilent Tech-

nologies) containing a C-terminal Myc tag and Kanamycin resistance. Human neuroblastoma SH-SY5Y cells were cultured in 6-well plates in DMEM/F12 medium until they were 80% confluent. On the day prior to transfection, medium was replaced with OPTI-MEM antibiotic and serum free media (Invitrogen) for 24 hours. The cells in each well were then transfected using Lipofectamine 2000 (Invitrogen) with 2 μg/well of pCMV-Tag5, pCMV-Tag5-CRMP2-T555A, pCMV-Tag5-CRMP2-T514A, pCMV-Tag5-CRMP2-T509A, pCMV-Tag5-CRMP2-S518A or pCMV-Tag5-CRMP2-S522A. Cells were then treated with Aβ peptides as described earlier. Cells were lysed and proteins were collected for immunoprecipitation and western immunoblotting.

Preparation of cell and tissue lysates for western blotting

Human neuroblastoma SH-SY5Y cells and brain tissues (AD, FTD, HD, MS, and NNDC) were lysed using cell lysis buffer (Cell Signaling Technology) containing 1% (v/v) protease and phosphatase inhibitors (Calbiochem) (**Table 1**). Cell lysates were centrifuged at 10,000 × *g* for 15 minutes at 4°C and the supernatants were collected. Protein concentrations were determined using the bicinchoninic acid (BCA) protein assay kit (Thermo Scientific, Waltham, MA, USA).

Immunoprecipitation

Immunoprecipitation was performed by adding 1 μg of mouse monoclonal anti-CRMP-2 antibody, to 100 μg of total protein from each sample. Samples were incubated overnight at 4°C followed by another overnight incubation with 100 μL of Protein G magnetic beads on a rotating wheel. Beads were separated using a magnetic stand (Merck Millipore, Darmstadt, Germany) and the supernatants were removed. Three washes were then performed with cell lysis buffer. Proteins were dissociated from the beads by heat at 95°C for 5 minutes in 1× sample loading buffer (Invitrogen) containing beta-mercaptoethanol. Electrophoresis of the samples was done using 4–12% Bis-Tris gels (Invitrogen).

Western immunoblotting

5 μg of total protein was loaded and run on a 4–12% Bis-Tris gel (Invitrogen). Proteins were then transferred onto polyvinylidene fluoride membranes (PVDF) (Millipore) and blocked with 5% skim milk powder in TBST for one hour at room temperature. The membranes were then incubated overnight at 4°C with following primary antibodies: mouse monoclonal anti-CRMP-2 (1:1000, Immuno-Biological Laboratories); anti-α-tubulin (1:5000, Millipore); anti-phospho-Thr555 CRMP-2 (1:5000); anti-phospho-Thr514 CRMP-2 (1:500, Cell Signaling Technology); anti-phospho-Ser522 CRMP-2 (1:2000, ECM Biosciences); anti-tau-5 (1:2000, Calbiochem); anti-FLAG (1:2000, Sigma-Aldrich); anti-kinesin light chain (KLC) (1:2000, Millipore) or anti-Myc (1:2000, Millipore). After three 10 minute washes with TBST, membranes were incubated with secondary anti-rabbit (1:10,000) or anti-mouse (1:10,000) HRP-conjugated antibodies diluted in TBST for 2 hours at room temperature. Proteins were detected using ECL prime chemiluminescence (GE Healthcare). The films were scanned using the Alpha Imager (Alpha Innotech) and the intensities of the bands were measured using ImageQuant TL v2003 software (Nonlinear Dynamics Ltd., Newcastle Upon Tyne, United Kingdom).

Plaque assay with human neuroblastoma SH-SY5Y cells

Autoclaved coverslips were placed in a 24-well plate. 10 μL of $A\beta_{1–40}$ peptide or $A\beta_{1–40}$ scrambled peptide at a concentration of 10 μM was dropped in the middle of the coverslips or plastic wells and were air dried overnight to form plaques. Cells were seeded at a density of 100,000 cells per well for wells or coverslips that had been treated with $A\beta_{1–40}$ peptide, or, at a density of 50,000 cells per well for wells or coverslips that had been treated with $A\beta_{1–40}$ scrambled peptide. Cells were treated with 10 μM retinoic acid in DMEM/F12 medium (Invitrogen) supplemented with 10% fetal bovine serum (Invitrogen) and 1% v/v penicillin/streptomycin (Invitrogen) for 24 hours. After three washes with PBS (Ca^{2+}, Mg^{2+}) (Invitrogen), the cells were fixed with 4% PFA for 10 minutes at room temperature. Cells were then stained with 0.002% (w/v) Thioflavin T for 30 minutes at room temperature, and followed by overnight incubation with monoclonal mouse anti-NF200 antibody (1:200) (Thermo Scientific, Waltham, MA, USA) and polyclonal rabbit anti-pCRMP2 antibody (1:200) prepared in PBS with 5% (v/v) normal goat serum (Invitrogen) and 0.2% (v/v) Triton-X100 (Sigma-Aldrich) at 4°C. After three washes with PBS, cells were stained with Alexa-Fluor 555 goat anti-rabbit IgG (1:200) (Thermo Scientific, Waltham, MA, USA) and Alexa-Fluor 488 goat anti-mouse IgG (1:200) (Thermo Scientific, Waltham, MA, USA) for 2 hours at room temperature. Coverslips were removed from the wells and mounted upside down onto slides with fluorescent mounting medium (Dako) while glycerol was added to plastic wells. Images were captured under an oil objective lens (60×) on a Nikon C1 Upright confocal microscope. The 16-bit images were converted to TIFF files using ImageJ software and formatted using Adobe Photoshop CS3 software. The percentage of pT555CRMP-2 positive SH-SY5Y cells was calculated by counting the number of pT555CRMP-2 positive SH-SY5Y cells and the overall number of cells from three fields inside and three different fields outside the plaque.

Mass spectrometry

The protein was reduced in 2.5 mM DTT at 50°C for 30 minutes followed by alkylation with 10 mM Iodoacetamide for 30 minutes in the dark at room temperature. Following alkylation, a solution containing 1 μg Trypsin (Promega, Madison, WI, USA) in 20 mM Ammonium bicarbonate was added and the samples were incubated at 37°C overnight. Tryptic digests were analyzed by LC-MS/MS using the QExactive mass spectrometer (Thermo Scientific) coupled online with a RSLC nano HPLC (Ultimate 3000, Thermo Scientific). Samples were concentrated on a 100 μm, 2 cm nanoviper pepmap100 trap column with loading buffer (2% acetonitrile, 0.1% Formic acid) at a flow rate of 15 μL/minute. The peptides then eluted and separated with a Thermo RSLC 50 cm pepmap100, 75 μm id, 10 nm pore size, reversed phase

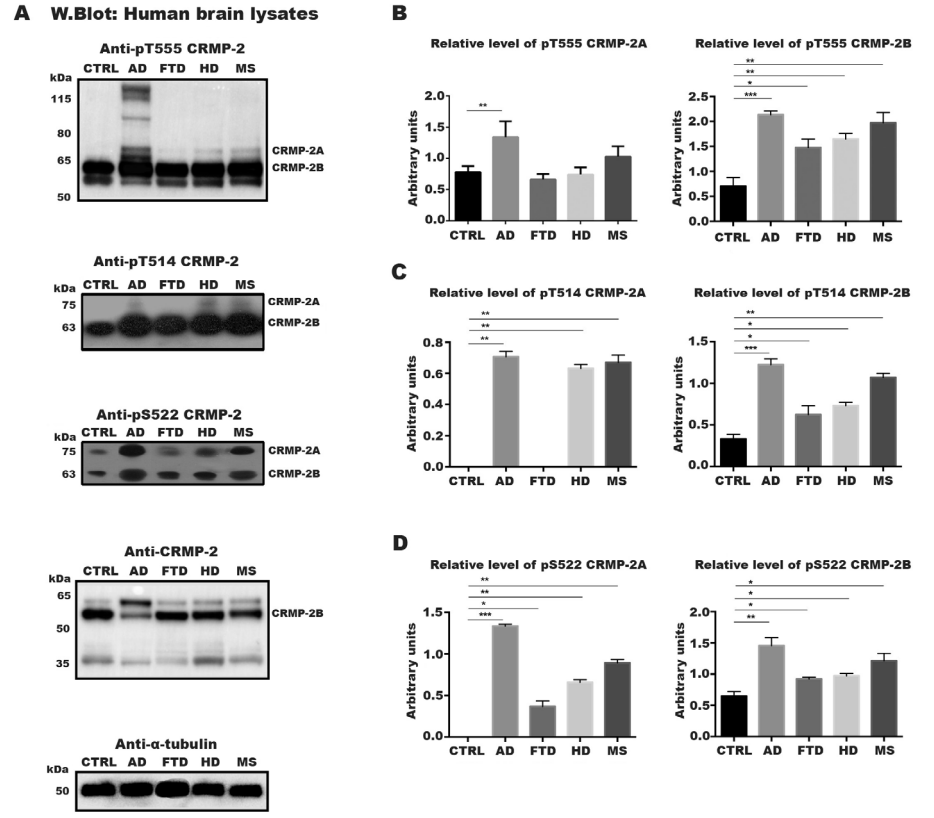

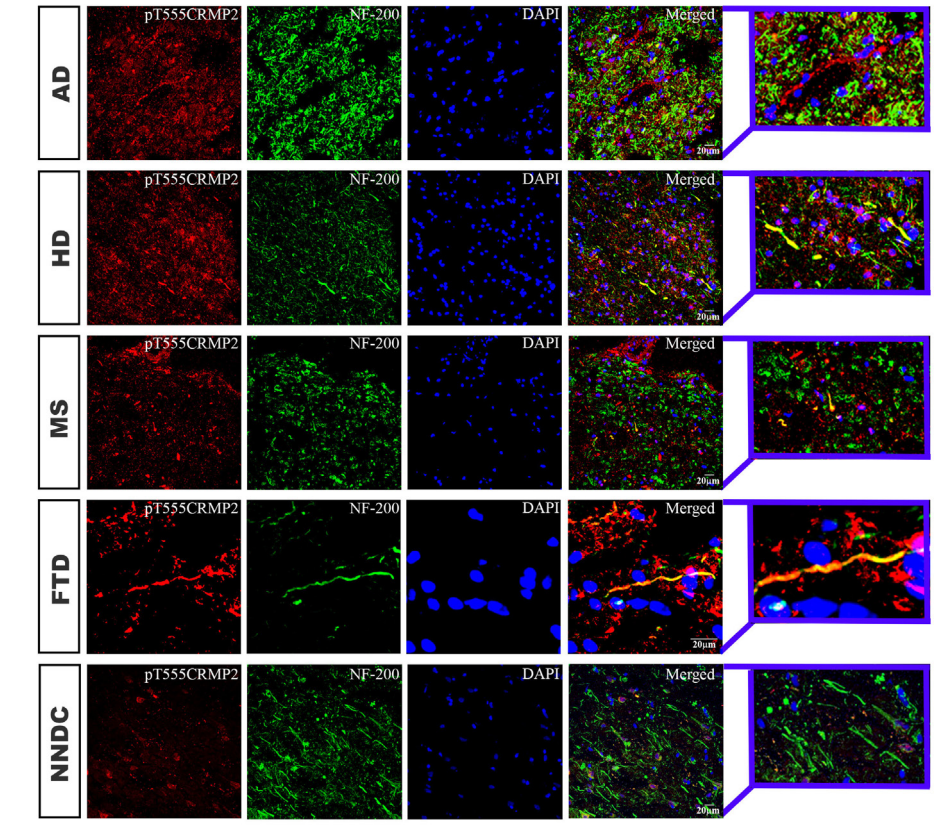

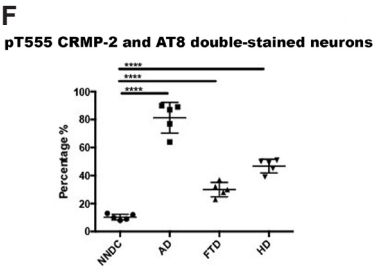

Figure 1 Elevated CRMP-2 phosphorylation levels are common in neurodegenerative diseases.

(A) Increased phosphorylation of CRMP-2 at Thr555, Thr514, and Ser522 sites are readily detected in AD (n = 8), FTD (n = 8), HD (n = 4), MS (n = 8) brain lysates when compared with non-neurological disease control (NNDC; n = 12) lysates. Regardless of the phosphorylation of all putative phosphorylated forms of CRMP-2 being present throughout the neurodegenerative diseases screened, the most abundant phospho-specific site during neurodegeneration was that of Thr555 and specifically enhanced in AD samples. (B) Increased levels of phosphorylated CRMP-2A (75 kDa) at the Thr555 site can be demonstrated for AD brain lysates; $^{**}P < 0.01$. Increased levels of phosphorylated CRMP-2B (62 kDa) at the Thr555 site, are also demonstrated in AD, HD and MS brain lysates ($^{*}P < 0.05$, $^{**}P < 0.01$, $^{***}P < 0.001$). (C) Further increased levels of phosphorylation CRMP-2A were demonstrated at the Thr514 site in AD, HD and MS brain lysates ($P < 0.01$). Similarly, increased levels of phosphorylated CRMP-2B at the Thr514 site was also demonstrated in AD, HD, and MS brain lysates ($^{*}P < 0.05$, $^{**}P < 0.01$, $^{***}P < 0.001$). (D) Increased levels of phosphorylated CRMP-2A were demonstrated at the Ser522 site in AD, HD and MS brain lysates ($^{*}P < 0.05$, $^{**}P < 0.01$, $^{***}P < 0.001$). In the same context, increased levels of phosphorylated CRMP-2B were also illustrated at the Ser522 site in AD, FTD, HD and MS brain lysates ($^{*}P < 0.05$, $^{**}P < 0.01$). (E) Immunofluorescent localization of pT555CRMP-2 to degenerative axons and neurons counterstained with NF200. Inset focused on dystrophic axons with intense expression of pT555CRMP-2. Scale bars: 20 μm. (F) Percentage of pT-555CRMP-2-AT8 double-labeled neurons. The graph shows significant differences in the percentage of pT555CRMP-2-AT8 double stained neurons of frozen sections obtained from NNDC (n = 8), AD (n = 4), FTD (n = 4), HD (n = 4) and MS (n = 4) patients compared to non-neurological disease control ($^{****}P < 0.0001$). Statistically significant differences were demonstrated following multiple pair-wise comparisons (one-way analysis of variance with Tukey's *post hoc* tests performed). AD: Alzheimer's disease; FTD: fronto-temporal dementia; HD: Huntington's disease; MS: multiple sclerosis; CTRL: non-neurological disease control brain tissue.

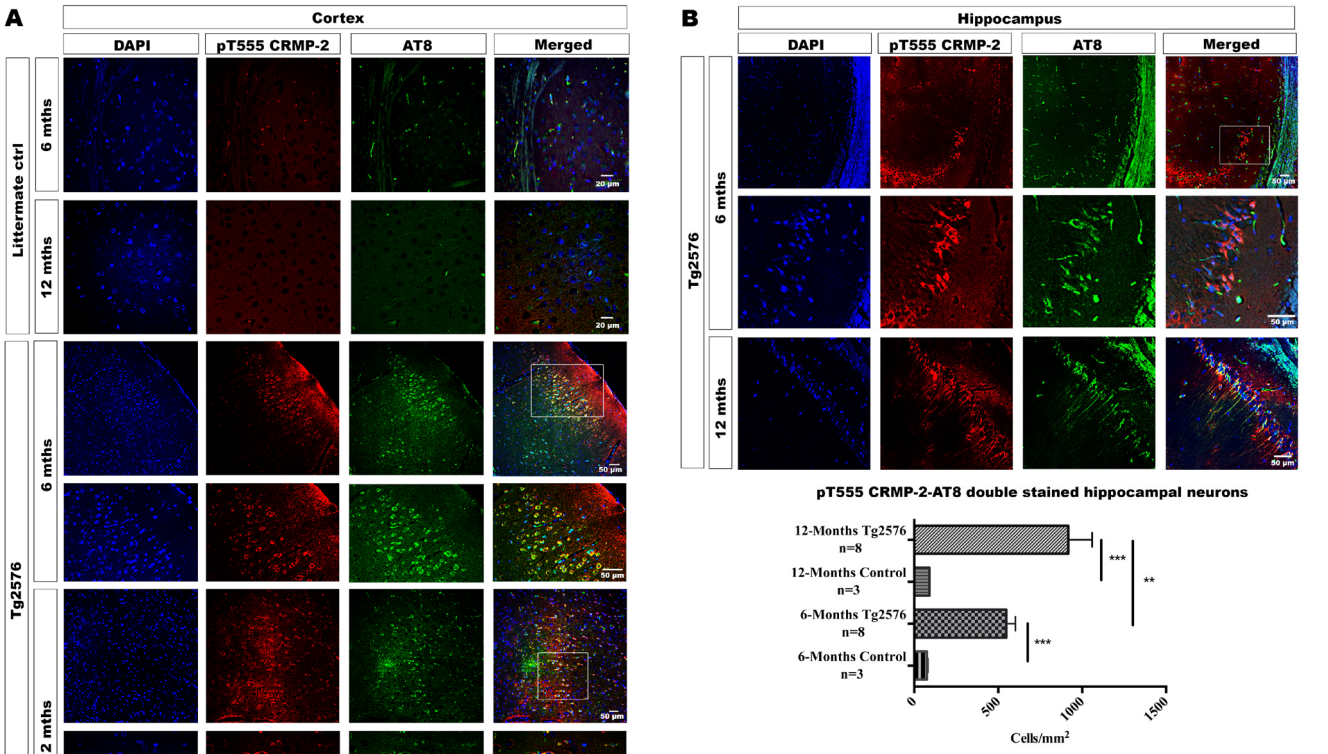

Figure 2 Elevated pThr555CRMP-2 and AT8 immunostaining of brain sections in the cortex and hippocampus of Tg2576 mice at 6 and 12 months of age.

(A) Lack of immunolabeling of pThr555-CRMP-2 and AT8 in cortical neurons of coronal paraffin brain sections from 6- and 12-month-old littermate control mice. Co-localization of pThr555-CRMP-2 with AT8 in degenerative cortical neuronal somata and axons of 6- and 12-month-old Tg2576 mice (inset). Quantification of pThr555-CRMP-2 and AT8 double-labeled cortical neurons illustrates an approximate 2-fold increase with the increase in age of the Tg2576 mice (n = 3 littermate control and n = 8 Tg2576 mice at 6 and 12 months old respectively, $^{**}P < 0.01$, $^{****}P < 0.0001$). (B) Co-localization of pThr555-CRMP-2 with AT8 in degenerative hippocampal neuronal somata and axons of 12-month-old Tg2576 mice (inset). Quantification of double-labeled hippocampal neurons also illustrates an approximate 2-fold increase with the increase in age of the Tg2576 mice (n = 3 littermate control and n = 8 Tg2576 mice at 6 and 12 months old respectively, $^{**}P < 0.01$, $^{***}P < 0.001$). Statistically significant differences were demonstrated following multiple pair-wise comparisons (one-way analysis of variance with Tukey's *post hoc* tests performed).

nano column with a 15 minute gradient of 90% buffer A (0.1% formic acid) to 40% B (80% acetonitrile, 0.1% formic acid) and to 95% buffer B in 10 minutes, at a flow rate of 300 nL/min. The eluant was nebulized and ionized using the Thermo nano electrospray source with a distal coated fused silica emitter (New Objective) with a capillary voltage of 1900 V. Peptides are selected for MSMS analysis in Full MS/dd-MS2 (TopN) mode with the following parameter settings: TopN 10, resolution 17500, MSMS AGC target 1e5, 60 ms Max IT, NCE 27 and 3 m/z isolation window. Underfill ratio was at 10% and dynamic exclusion was set to 15 seconds.

Data from LCMSMS run was processed using proteome discoverer V1.4 (Thermo Scientific) and searched against a custom database comprising proteome datasets downloaded from the Uniprot web site (http://www.uniprot.org/) using the MS Amanda search engine. The following search parameters were used: missed cleavages, 1; peptide mass tolerance, ± 15 ppm; peptide fragment tolerance, ± 0.2 Da; peptide charge, 2+, 3+ and 4+; static modifications, carbamidomethyl; Dynamic modification, oxidation (Met). Low and medium confidence peptides were filtered with at least 0.02 FDR (high confidence).

Statistics

Data were analyzed using GraphPad Prism v6.0 software (GraphPad software, La Jolla, CA, USA). A two-tailed Student's t-test or a one-way analysis of variance (ANOVA), for multiple pair-wise comparisons with non-parametric Tukey's *post-hoc* tests, based on normality of the data (determined by the Kolomogorov Smirnov tests), were performed to determine statistical significance between groups. Significance was defined as $P < 0.05$ at a 95% confidence level.

Results

CRMP-2 phosphorylation is increased in human brain lysates from donor individuals with AD

To define the specific CRMP-2 phosphorylation events oc-

curring in post-mortem AD samples, western blot analysis was performed on AD temporal and frontal lobe cortical samples, then compared with other non-inflammatory and inflammatory neurodegenerative diseases that included HD (caudate nucleus samples), secondary progressive MS (periventricular white matter lesion samples), FTD (cortical samples), along with brain samples from non-neurological disease controls (acute cardiac arrest). The data show that primarily in AD, and to a certain degree in the other neurodegenerative diseases, the brain lysate samples exhibited phosphorylation at the pT555 of the major isoform, CRMP-2B (62 kDa) (**Figure 1A** & **C**). However, the phosphorylation of the alternatively spliced variant (75 kDa) CRMP-2A, at this T555 site, was significantly enhanced primarily in AD (**Figure 1A** & **B**). We also found increases in the other putative phosphorylation sites for CRMP-2 in AD, FTD, HD and MS patients, namely, pT514CRMP-2A, pT514CRMP-2B, pS522CRMP-2A and pS522CRMP-2B (**Figure 1A–D**). These data may suggest that CRMP-2 undergoes hyperphosphorylation during neurodegeneration regardless of whether peripheral inflammatory mechanisms are operative.

Co-labeling experiments performed on paired frozen human brain tissue

To confirm that the phosphorylated form of CRMP-2 was co-localized with hyperphosphorylated tau within degenerative neurons, immunohistochemical staining of frozen sections was performed for the AD, FTD, MS, HD and NNDC paired brain samples obtained from the western blot experiments (**Figure 1**). We found increased labeling of pT555-CRMP-2 localized to AT8-positive degenerative neurons (**Figure 1E)**. Quantification of the double stained neurons illustrates significant increases in pT555CRMP-2-positive degenerative neurons in AD, FTD and HD cortex as compared to NNDC (**Figure 1F**). Also, quantification of the double stained axons shows a significant increase in pT555CRMP-2 within MS white matter compared to NNDC (**Figure 1F**). This finding provides evidence that neurodegeneration exhibits common molecular pathways that drive neuronal dysfunction and axonal dystrophy and that pT555CRMP-2 is prominent amongst these degenerative neurons.

Increased levels of pT555-CRMP-2 are observed in neurons undergoing degeneration in the cortex and hippocampus of Tg2576 transgenic mice

We have previously reported that the phosphorylation of CRMP-2 occurs in the brains of Tg2576 mice as they age, correlating with the increase in Rho-A-GTP levels, a consequence of decreased Rac1-GTP activity (Petratos et al., 2008). We now posed the question whether this phosphorylated form of CRMP-2 was specific to neurons that were degenerating in the transgenic mouse brain. At 6 months of age (when initial cognitive deficits have been reported to appear (Westerman et al., 2002)), and 12 months of age (when substantial amyloid plaques along with cognitive decline are present), we found increased labeling of pT555-CRMP-2 localized to neurons exhibiting abnormal hyper-phosphorylated tau (**Figure 2A**). This was observed specifically in degenerating neuronal somata and neurites within the cortices (**Figure 2A**) and hippocampi (**Figure 2B**) of Tg2576 mice. Occasionally, we also observed double-labeled cortical neurons for pT555-CRMP-2 and AT8 in Tg2576 mice at 6 months of age (n = 5) (**Figure 2A**) but generally as degeneration progressed (by 12 months of age) in the cortices and hippocampi, the pT555 CRMP-2 levels were profoundly increased (**Figure 2A** & **B**). These data demonstrate that pT555 CRMP-2 levels were increased in AT8-positive degenerative cortical and hippocampal neurons of the APP mutant Tg2576 mice (Fassas et al., 2002) under increased Aβ load in the brain (**Table 2**).

Altered neurite morphology in SH-SY5Y human neuroblastoma neurons develop near an Aβ-substrate in culture

In an attempt to investigate the effect of amyloid plaques on neurite elongation and CRMP-2 phosphorylation, we established SH-SY5Y cultures as they were growing neurites but cultured on a centrally placed Aβ-deposit (laboratory made APs as a substrate) in a 24-well culture plate. The cells that attached and grew directly on the artificial 'AP' and the cells that grew adjacent to it displayed dystrophic neurites (**Figure 3A**; arrowhead) with numerous varicosities (**Figure 3A**; arrow). On the other hand, the axons of the cells that were growing away from the plaque grew in a more linear trajectory (**Figure 3A**). This is very different from the cells attached to a scrambled sequence of the Aβ peptide artificial 'plaque' where the cells are visibly healthy and the axons grow straight through the edge of the artificial 'plaque' (**Figure 3A**). These results suggest signaling deficits affecting the neuronal cytoskeleton effective at the active growth zones of neurites.

To examine the relationship between CRMP-2 phosphorylation at T555 site and dystrophic neurites, immunocytochemical staining of SH-SY5Y cells with pT555 CRMP-2 and NF200 was performed. After adding the cells into wells containing an artificial 'amyloid plaque', cells that were attached to the plaque or growing near to the plaque showed dystrophic neurites with substantial staining with pT555 CRMP-2 (**Figure 3B**; arrowhead). However, the cells that were growing away from the plaque showed less pT555 CRMP-2 staining at the neurites. Similarly, the cells that were growing inside the scrambled peptide substrate-containing wells showed vastly reduced pT555 CRMP-2 neuronal staining (**Figure 3B**). This was enumerated to illustrate these findings with ~80% of SH-SY5Y cells growing upon or near the Aβ substrate expressing pT555CRMP-2 whereas only ~20% of the cells that had grown outside from the artificial plaque expressed these levels. These data illustrate that neuronal interactions with insoluble Aβ may potentiate the phosphorylation of CRMP-2 at the T555 site.

Soluble Aβ preferentially increases CRMP-2 phosphorylation in SH-SY5Y neuroblastoma cells at the T555 site

Since generation of neurotoxic species of Aβ is characteristic of AD, we investigated the initial effects of $A\beta_{1–40}$ and $A\beta_{1–42}$ on phosphorylation of CRMP-2 in differentiated SH-

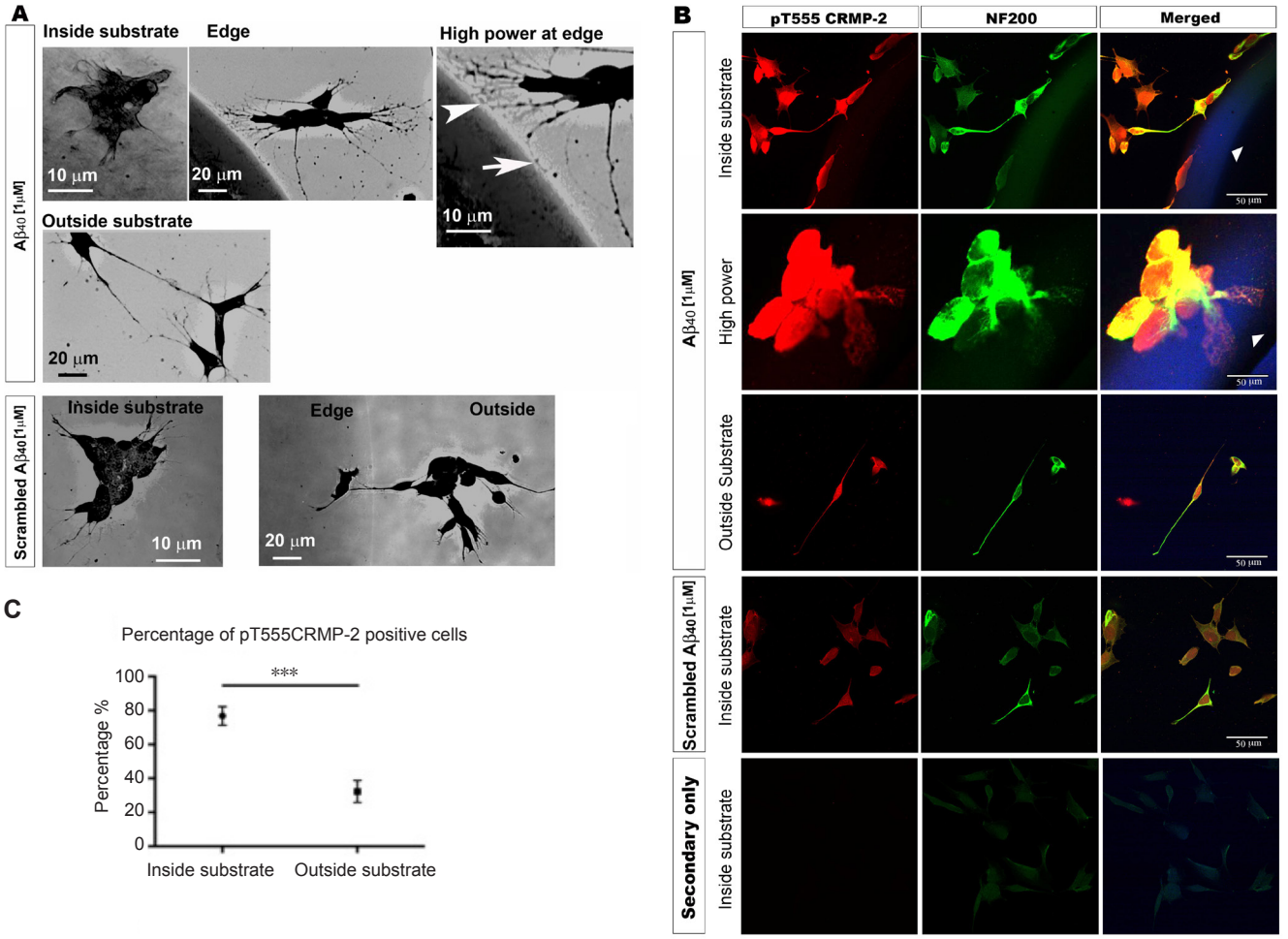

Figure 3 Altered neurite morphology in SH-SY5Y human neuroblastoma cells within or near amyloid plaques (APs).
(A) A laboratory made 'AP' centrally located on a 10 cm diameter glass coverslip, is placed at the bottom of a 24 well plate, then seeded with 100,000 cells per well. Those cells that had grown inside or near the 'AP' exhibit substantial neurite curvature (arrowhead) or dystrophic neuritic swellings. Furthermore, neurites growing toward the 'AP' edge also show enlarged varicosities (A; arrow). However, the SH-SY5Y cells that grow away from the artificial 'AP' substrate exhibit linear neurite formation. Alternatively, the SH-SY5Y cells that were cultured within or near the scrambled Aβ peptide artificial 'APs', do not exhibit dystrophic neurite formation. The cells appear unrestricted and the neurites grow in a linear fashion through the artificial 'AP'. (B) SH-SY5Y cells cultured in wells with an artificial 'AP' were immunostained for pT555-CRMP-2 and NF200. The cells that attached directly to the 'AP' or grew near it show substantial staining with pT555 CRMP-2 along with neurite dystrophy (arrowhead). While the cells that grew outside the substrate exhibit linear neurites with basal levels of pT555 CRMP2 immunostaining. The cells that grew within the scrambled Aβ peptide 'AP' demonstrate neuritogenesis with less pT555 CRMP-2 immunostaining. (C) Percentage of pT555CRMP-2 positive SH-SY5Y cells inside *vs.* outside the artificially made 'AP'. The graph shows significant difference in the percentage of pT555CRMP-2 stained SH-SY5Y cells that surround the artificial AP, compared to the cells that are outside the AP ($n = 3$ independently assessed wells per condition, at least $n = 100$ SH-SY5Y cells counted either inside or outside the artificial plaque; ***$P < 0.001$). This statistically significant difference was demonstrated following a two-tailed Student's t test under a normal distribution.

SY5Y human neuroblastoma cells. Prior to delineating these downstream signal transduction effects exerted by variable concentrations of $A\beta_{1–40}$ and $A\beta_{1–42}$ species, $A\beta_{1–40}$ and $A\beta_{1–42}$ treatment of cultured SH-SY5Y cells were imaged either by confocal microscopy or atomic force microscopy (AFM) of the aggregation of $A\beta_{1–42}$ species. Fluorescently-tagged $A\beta_{1–40}$ (Fluor 488-labeled $A\beta_{1–40}$) demonstrated localization of small molecular weight species directly onto the cholera toxin B subunit (Alexa fluor-555 tagged)-labeled plasma membrane subdomains of differentiated SH-SY5Y cells (**Figure 4A**). However, $A\beta_{1–42}$ could only be imaged under these defined medium conditions using powerful AFM of this species' fast aggregation (**Figure 4B**).

We found that the phosphorylation of CRMP-2A (75 kDa) and CRMP-2B (62 kDa) at the T555 site was elevated in correlation to increases in the extracellular concentration of $A\beta_{1–40}$ administration (**Figure 4C** & **E**). However, we found decreased phosphorylation of CRMP-2A and CRMP-2B upon $A\beta_{1–42}$ treatment of these cells (**Figure 4C** & **E**). Intriguingly, we identified a 55 kDa immunoreactive band (**Figure 4C;** arrow). We subsequently immunoprecipitated CRMP-2 using the monoclonal antibody (IBL) and after in-gel digestion, processed this band for identification through mass spectrometry (LCMS). We identified the band to be the C-terminal 55 kDa cleaved product of CRMP-2 as previously reported in Prion disease (Shinkai-Ouchi et al., 2010) and acquired brain injury samples (Zhang et al., 2007) (see **Additional Table 1**). These data support other putative post-translational modifications to CRMP-2 such as calpain cleavage that has been reported as a major downstream event occurring in neuronal cell death (Zhang et al., 2007).

Despite readily detectable elevation in CRMP-2 phosphor-

Table 1 Post-mortem human brain tissue (freshly frozen in liquid nitrogen)

Age (years)	Gender	PMI (hours)	Diagnosis
65.1	Female	12.0	MS/AD
38.5	Male	25.0	MS
66.2	Male	18.5	MS
71.4	Male	24.0	MS
49.9	Male	13.0	MS
62.7	Female	26.0	MS
49.9	Male	26.5	MS
51.1	Male	22.0	MS
71.4	Male	9.5	AD
73.0	Male	9.5	AD
83.8	Male	10.0	AD
88.4	Female	11.0	AD
78.0	Male	20.0	AD
78.0	Female	19.5	AD
60.0	Male	13.5	AD
60.6	Male	12.0	FTDu
61.4	Female	20.5	FTDu
77.0	Male	6.0	FTDu
66.8	Male	27.0	FTDu
40.0	Male	18.5	FTDu
72.0	Female	11.0	FTDu
76.0	Male	6.0	FTDu
69.0	Female	21.5	FTDu
61.1	Male	17.0	HD
66.7	Female	18.5	HD
57.2	Female	22.0	HD
72.2	Female	22.0	HD
52.1	Male	23.0	Control
82.7	Male	27.0	Control
63.4	Female	20.5	Control
63.9	Male	21.5	Control
73.6	Male	19.0	Control
73.0	Female	26.5	Control
48.0	Male	20.0	Control
49.9	Male	7.5	Control
83.6	Female	16.0	Control
78.8	Female	19.0	Control
57.6	Male	20.5	Control
73.5	Male	22.0	Control

Post-mortem interval (hours); MS: multiple sclerosis; AD: Alzheimer's disease; HD: Huntington's disease; FTD: fronto-temporal dementia; control: non-neurological disease control brain tissue.

Table 2 Levels of Aβ in the brain of Tg2576 transgenic mice determined by ELISA

Aβ isoform	6 months	12 months	18 months
$Aβ_{1–40}$	1.25	2.25	3.25
$Aβ_{1–42}$	12	14	15

Table 3 cDNA of human CRMP-2

Construct	Mutation	Phosphorylation site abolished
CRMP-2 T555A	Thr-555 into Ala-555	ROCKII
CRMP-2 T509A	Thr-509 into Ala-509	GSK-3β
CRMP-2 T514A	Thr-514 into Ala-514	GSK-3β
CRMP-2 S518A	Ser-518 into Ala-518	GSK-3β
CRMP-2 S522A	Ser-522 into Ala-522	Cdk-5

ylation at the T555 site, no differences were detected in the phosphorylation of CRMP-2 at the Thr514 and Ser522 sites (**Figure 4C, F** & **G**). These results demonstrate that the phosphorylation of CRMP-2 predominantly increases with elevated extracellular levels of $Aβ_{1–40}$ (**Figure 4C**). Furthermore, we found that CRMP-2 phosphorylation at the T555 site correlated with increased levels of hyperphosphorylated tau (AT8) upon elevated $Aβ_{1–40}$ concentrations (**Figure 4C** & **H**).

Treating the cells with the scrambled form of the Aβ peptide had no effect on the levels of CRMP-2 or tau phosphorylation (**Figure 4D** & **H**). Despite the difference in post-translational modification of CRMP-2 by $Aβ_{1–40}$ and $Aβ_{1–42}$ treatment of differentiated SH-SY5Y cells (*i.e.*, phosphorylation versus cleavage, respectively) both species could equally reduce neurite length when compared to their scrambled peptide counterparts (**Figure 4I**). These data suggest that CRMP-2 phosphorylation at T555 site is an $Aβ_{1–40}$-dependent mechanism, which results from small molecular weight species binding to neuronal plasma membrane microdomains and effect neurite outgrowth. $Aβ_{1–40}$-dependent cleavage of CRMP-2 can also elicit the similar biological outcome.

Expression of the phospho-mutantT555A CRMP-2 construct in SH-SY5Y neuroblastoma cells promotes neurite elongation even in the presence of extracellular Aβ

To define whether phosphorylation of CRMP-2 at the T555 site is the dominant molecular event responsible for Aβ-induced neurodegeneration, or alternative CRMP-2 phosphorylation events can also contribute to neurite outgrowth inhibition, SH-SY5Y cells were transiently transfected with flag and myc-tagged T555A (Rho-kinase site) CRMP-2 phospho-mutant construct, then administered 10 μM of $Aβ_{1–40}$ for 24 hours (**Table 3**). The cells were fixed and then immunostained with anti-NF200 and anti-Flag antibodies to demonstrate their ability for neurite outgrowth even in the presence of Aβ. Cells transfected with the T555A cDNA were able to form long thick neurites (**Figure 5A**; arrow), even though endogenous phosphorylation of CRMP-2 was demonstrated in the presence of Aβ (**Figure 5B**). However, the T555A mutant transfected SH-SY5Y cells demonstrated neurite length integrity in the presence of Aβ (**Figure 5C**). These results demonstrate that the limiting Aβ-dependent phosphorylation of CRMP-2 at the T555 site plays a central role in the preservation of neurite integrity.

Effect of Aβ on kinesin and tubulin binding to CRMP-2 in SH-SY5Y neuroblastoma cells

Since we determined that the major Aβ-dependent phosphorylation of CRMP-2 was at the T555 site in SH-SY5Y

cells, we decided to investigate whether this CRMP-2 phosphorylation had the ability to dissociate kinesin and tubulin. We used undifferentiated SH-SY5Y cells (control, no retinoic acid), differentiated SH-SY5Y cells were treated with retinoic acid, SH-SY5Y cells were treated with $A\beta_{1–40}$ at three different concentrations [0.5, 1.0 and 10.0 μM] and finally SH-SY5Y cells were treated with $A\beta_{1–42}$ at three different concentrations [0.5, 1.0 and 10.0 μM]. To identify the interaction between the CRMP-2/tubulin/kinesin multimeric complex, we immunoprecipitated CRMP-2 from cell lysate samples following administration of the above described Aβ concentrations and control experiments. Following western blotting, the membranes were probed with either the monoclonal anti-KLC-1 or monoclonal anti-α-tubulin. We found that CRMP-2-bound kinesin and tubulin were reduced with the increase in the concentration of $A\beta_{1–40}$ and $A\beta_{1–42}$ administered, compared to untreated control cells and cells treated with scrambled peptide (**Figure 6**). These data suggest that $A\beta_{1–40}$ and $A\beta_{1–42}$ can affect the ability of CRMP-2 to bind to tubulin heterodimers (soluble) and kinesin.

Expression of T555A CRMP-2 in SH-SY5Y neuroblastoma cells improves CRMP-2 association with kinesin and tubulin in the presence of Aβ

Important physiological roles that have been attributed to CRMP-2 include the binding of alpha-and beta-tubulin heterodimers, to facilitate their transport to the plus-ends of microtubules as a means of promoting neurite extension (Fukata et al., 2002). In addition, the association of CRMP-2 with kinesin-1, the microtubule motor protein complex (Szpankowski et al., 2012), can facilitate vesicular anterograde axonal transport (Kimura et al., 2005). We transiently transfected SH-SY5Y cells with flag-and myc-tagged CRMP-2 phospho-mutant constructs; T555A (Rho-kinase site), T509A, T514A, S518A (GSK-3β sites) and S522A (Cdk5 site). The cells were treated with $A\beta_{1–40}$ or $ScrA\beta_{1–40}$ [10 μM] for 24 hours. CRMP-2 was immunoprecipitated using an anti-CRMP-2 monoclonal antibody (IBL) and then the level of CRMP-2-bound tubulin and kinesin was determined by western blotting using either anti-α-tubulin or anti-KLC antibodies. We detected elevated levels in CRMP-2-bound kinesin in T555A transfected SH-SY5Y cells. Cells that were transfected with either of the other constructs exhibited reduction in kinesin-association that could be a result of endogenous phosphorylation of CRMP-2 at the T555 site following $A\beta_{1–40}$ treatment (**Figure 7A** & **C**). We also found increased levels in CRMP-2-bound tubulin in T555A transfected SH-SY5Y cells (**Figure 7A** & **B**). Cells that were transfected with the other constructs showed decreases in the levels of tubulin association (**Figure 7A** & **B**) that again may well represent the endogenous phosphorylation of CRMP-2 at T555 site following $A\beta_{1–40}$ treatment. It is important to note that the levels of tubulin and kinesin that were bound to CRMP-2 did not decrease in the presence of $A\beta_{1–40}$ scrambled peptide (control peptide administration experiment) (**Figure 7A**–**C**). These data support the hypothesis that Aβ causes a reduction in neurite length and axonal transport through the phosphorylation of CRMP-2 at the T555 site by reducing its capacity to bind tubulin and kinesin.

Discussion

In this study, we have investigated how extracellular Aβ regulates CRMP-2 phosphorylation to induce neuritic abnormalities. We showed that Aβ-dependent neurite growth inhibition and axonal transport is due to the dysregulated association of CRMP-2 with the kinesin axonal motor protein complex. Furthermore, we show that CRMP-2-bound KLC-1 is reduced in brain lysates from patients with neurodegenerative disease, including AD. Moreover, we show that blockade of CRMP-2 phosphorylation restores kinesin association and neurite growth integrity. Collectively, these data suggest that Aβ-mediated neurodegeneration is initiated through the dysregulation of CRMP-2 binding to tubulin and kinesin. Hence, novel therapeutics could target this interaction in the quest to limit cognitive decline in AD.

It is now well documented that cognitive decline occurring in both familial and sporadic Alzheimer's disease (AD) is brought about through the aberrant processing of APP, seeding neurotoxic oligomeric species of Aβ that can promote de-afferentation of neurons. Recently, a receptor for oligomeric Aβ has been defined as the PrPC with a tangible signal transduction mechanism proposed to play a role in excitotoxic damage (Um et al., 2012). However, the downstream signaling of oligomeric Aβ leading to disorganization of the neuronal cytoskeleton along with its communication pathways remains to be elucidated. In this study, we have focused on how extracellular Aβ can disrupt important neuronal anterograde transport machinery to amplify the neurodegenerative process.

Vesicular transport requires an intact microtubule cytoskeleton (Oriola et al., 2015) (for review see Bressloff and Levien (2015) or Hirokawa and Takemura (2005)). Microtubules are stabilized by the tau protein, which has been shown to dissociate from microtubules in AD and FTD (Gustke et al., 1992). Although the hyperphosphorylation of tau is a pathological hallmark seen in AD and other neurodegenerative disorders, its etiologic involvement in the degenerative effects on synapses and neuritic dystrophy is still debated. Oligomeric Aβ has been shown to disrupt the microtubule cytoskeleton and cause neuritic dystrophy from the postsynaptic density (Zempel et al., 2010; Jin et al., 2011). In this study, we detected a significant increase in the phosphorylation of CRMP-2 at the T555 site in AD cortical lysates but to a lesser degree from other neurodegenerative disorders (HD and progressive MS) when compared with brain lysates from non-neurological disease controls, possibly suggesting Aβ-dependent phosphorylation of CRMP-2 occurs preferentially at this site.

It has been posited that phosphorylated CRMP-2 modifications can accumulate with the Wiskott-Aldrich syndrome protein family verprolin-homologous protein (WAVE1), in the post-mortem brain tissue of individuals with AD and 3xTg-AD mice (including the APP Swedish, MAPT P301L, and PSEN1 M146V mutations) that developed neu-

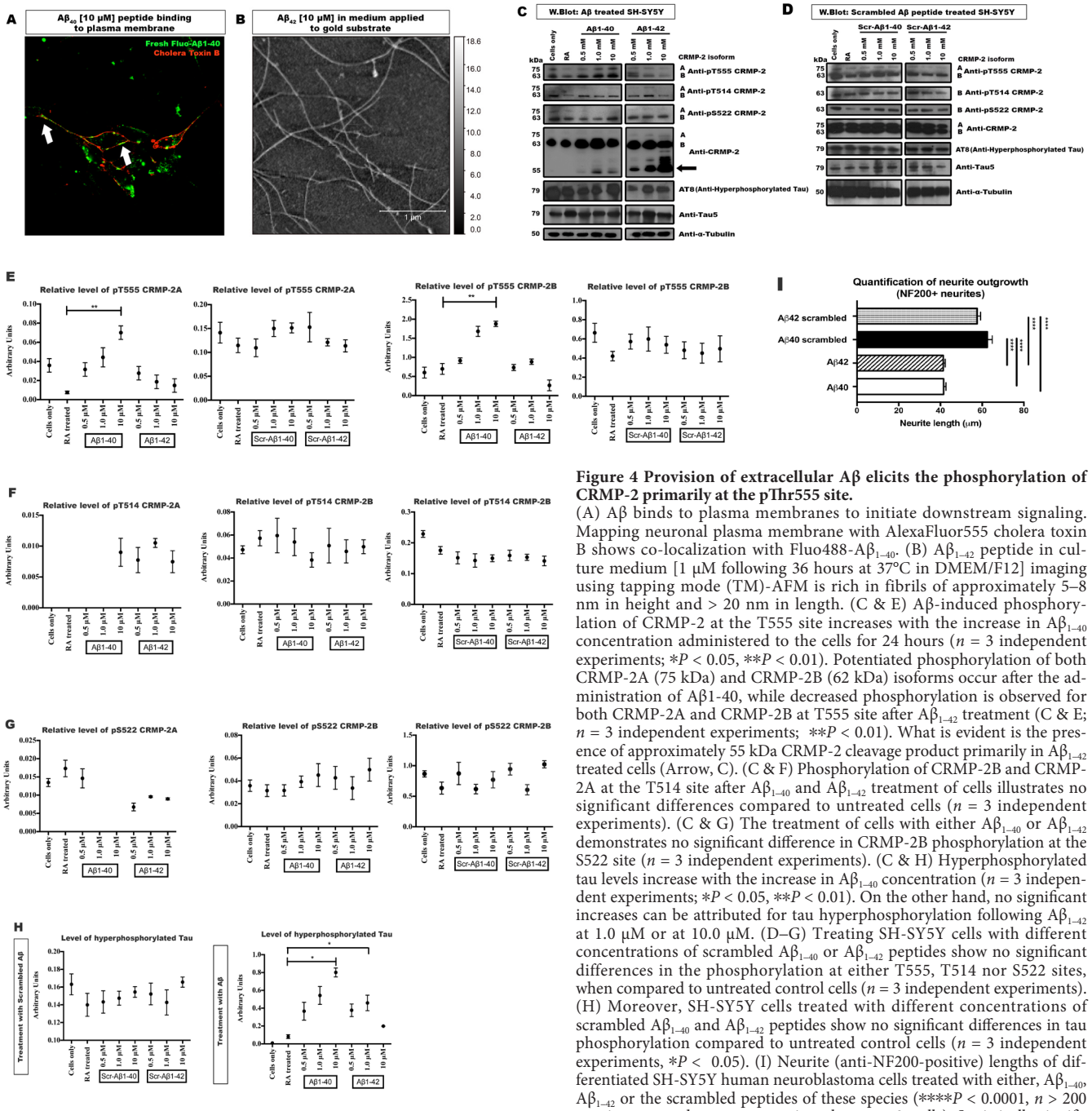

Figure 4 Provision of extracellular Aβ elicits the phosphorylation of CRMP-2 primarily at the pThr555 site.

(A) Aβ binds to plasma membranes to initiate downstream signaling. Mapping neuronal plasma membrane with AlexaFluor555 cholera toxin B shows co-localization with Fluo488-$Aβ_{1–40}$. (B) $Aβ_{1–42}$ peptide in culture medium [1 μM following 36 hours at 37°C in DMEM/F12] imaging using tapping mode (TM)-AFM is rich in fibrils of approximately 5–8 nm in height and > 20 nm in length. (C & E) Aβ-induced phosphorylation of CRMP-2 at the T555 site increases with the increase in $Aβ_{1–40}$ concentration administered to the cells for 24 hours (n = 3 independent experiments; $*P < 0.05$, $**P < 0.01$). Potentiated phosphorylation of both CRMP-2A (75 kDa) and CRMP-2B (62 kDa) isoforms occur after the administration of Aβ1-40, while decreased phosphorylation is observed for both CRMP-2A and CRMP-2B at T555 site after $Aβ_{1–42}$ treatment (C & E; n = 3 independent experiments; $**P < 0.01$). What is evident is the presence of approximately 55 kDa CRMP-2 cleavage product primarily in $Aβ_{1–42}$ treated cells (Arrow, C). (C & F) Phosphorylation of CRMP-2B and CRMP-2A at the T514 site after $Aβ_{1–40}$ and $Aβ_{1–42}$ treatment of cells illustrates no significant differences compared to untreated cells (n = 3 independent experiments). (C & G) The treatment of cells with either $Aβ_{1–40}$ or $Aβ_{1–42}$ demonstrates no significant difference in CRMP-2B phosphorylation at the S522 site (n = 3 independent experiments). (C & H) Hyperphosphorylated tau levels increase with the increase in $Aβ_{1–40}$ concentration (n = 3 independent experiments; $*P < 0.05$, $**P < 0.01$). On the other hand, no significant increases can be attributed for tau hyperphosphorylation following $Aβ_{1–42}$ at 1.0 μM or at 10.0 μM. (D–G) Treating SH-SY5Y cells with different concentrations of scrambled $Aβ_{1–40}$ or $Aβ_{1–42}$ peptides show no significant differences in the phosphorylation at either T555, T514 nor S522 sites, when compared to untreated control cells (n = 3 independent experiments). (H) Moreover, SH-SY5Y cells treated with different concentrations of scrambled $Aβ_{1–40}$ and $Aβ_{1–42}$ peptides show no significant differences in tau phosphorylation compared to untreated control cells (n = 3 independent experiments, $*P <$ 0.05). (I) Neurite (anti-NF200-positive) lengths of differentiated SH-SY5Y human neuroblastoma cells treated with either, $Aβ_{1–40}$, $Aβ_{1–42}$ or the scrambled peptides of these species ($****P < 0.0001$, n > 200 neurites counted per treatment in at least n = 3 wells). Statistically significant differences were demonstrated following multiple pair-wise comparisons (one-way analysis of variance with Tukey's *post hoc* tests performed).

rofibrillary tangles and Aβ plaques (Takata et al., 2009). The importance of this is still to be elucidated. However, since WAVE is a chief signalling protein for actin organization and binds with unphosphorylated CRMP-2 when it is being transported to axonal growth cones (Kawano et al., 2005b), the accumulation of WAVE with pCRMP-2 in AD brains was proposed to be a finding pertinent to synaptic deficits exhibited in the disease with increasing Aβ burden and tau accumulation (Takata et al., 2009).

We also detected a significant increase in the phosphorylation of CRMP-2 at the T514 and S522 sites in AD, HD, and MS brain lysate samples suggesting that hyperphosphorylation of this protein occurs during inflammatory and non-inflammatory neurodegeneration, irrespective of the Aβ load in the brain. Our cell culture analysis demonstrated significant increases in tau hyperphosphorylation with elevated extracellular $Aβ_{1–40}$ concentrations, corresponding to the elevation of CRMP-2 phosphorylation along with tubulin and kinesin-1 dissociation. Both the phosphorylation of CRMP-2 and the hyperphosphorylation of tau were found to occur in degenerating neurons of the hippocampus and cortex in the aging Tg2576 mouse brain when the Aβ load in

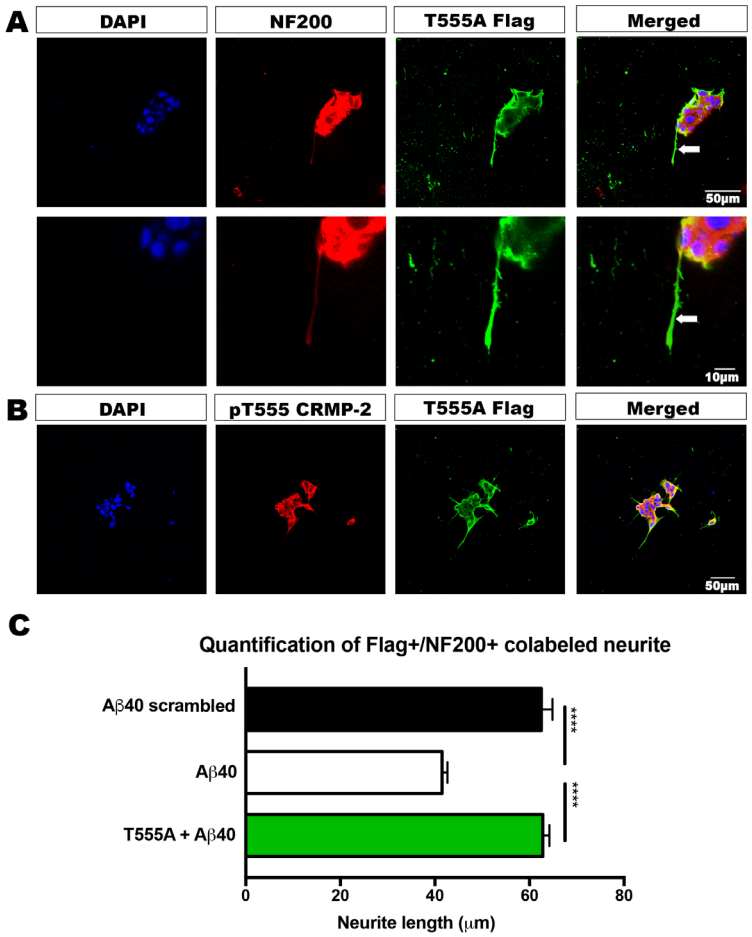

Figure 5 Immunostaining of $A\beta_{1-40}$ treated SH-SY5Y cells transfected with phospho-specific mutant constructs of Flag-tagged collapsin response mediator protein-2 (CRMP-2).
(A) SH-SY5Y cells transfected with the T555A CRMP-2 mutant construct and treated with 10 µM of $A\beta_{1-40}$ for 24 hours in culture. Anti-Flag positive labeling is distributed throughout the axon and neuronal soma co-labeled for NF200 (neuronal soma). Importantly, cells transfected with the T555A CRMP-2 mutant construct were able to produce long thick neurites (arrow), even following the treatment of these cells with 10 µM $A\beta_{1-40}$ for 24 hours in culture. (B) Anti-Flag-positive labeling is distributed throughout the axon and neuronal soma, with endogenous pThr555CRMP-2 expression (neuronal soma), after $A\beta_{1-40}$ treatment. Localization of pThr555CRMP-2 within the neuronal soma can also be observed. (C) Cells transfected with the phospho-specific T555A CRMP-2 mutant construct show Flag- and NF200-immunopositive neurite lengths in the presence of extracellular $A\beta_{1-40}$ (****$P < 0.0001$). Statistically significant differences were demonstrated following multiple pair-wise comparisons (one-way analysis of variance with Tukey's *post hoc* tests performed).

the brain was highest. Recently, it was reported that elevated phosphorylation of CRMP-2 at the T514 (GSK3β) site can be observed in post-mortem brain tissue of Lewy body dementias (LBD) associated with the Alzheimer's (Aβ plaque burden) high burden type and not related to the tauopathy and α-synuclein form of Parkinson's disease (Xing et al., 2016). Together these findings are consistent with the notion that tau hyperphosphorylation and CRMP-2 phosphorylation are most likely Aβ-dependent mechanisms governing AD-specific neurodegeneration.

Our data has identified that the increase in pT555-CRMP-2 levels could be localized in degenerative neurons with hyperphosphorylated tau both in AD cortical tissue and the Tg2576 mouse brains. These elevated levels in pT555-CRMP-2 and hyperphosphorylated tau were demonstrated in cultured SH-SY5Y cells following Aβ treatment. The link between tau and CRMP-2 posttranslational modifications initiating microtubule destabilization during neurodegeneration (in particular AD) has been eloquently described in a recent review by Hensley and Kursula (2016). These authors articulate the similarities of kinase-dependent phosphorylation on both of these microtubule-associated proteins (MAPs) but also highlight the differences that include the physiological role of CRMP-2 in anterograde transport of key growth-related proteins and receptors chief to the stability of the distal axon and synapse. This particular role of CRMP-2 is effected either through phosphorylation of its C-terminus or in fact by calpain-dependent cleavage to manifest dystrophic axons or dendrites. This would suggest that CRMP-2 is an important druggable target for AD (Hensley and Kursula, 2016).

While we demonstrated that $A\beta_{40}$ administration *in vitro* enhanced the phosphorylation status of CRMP-2, we also identified that $A\beta_{42}$ enhanced the cleavage of CRMP-2 in SH-SY5Y cells, which also limited its association with kinesin-1. In fact, the recent identification of axonal dystrophy being governed by calpain-mediated cleavage of CRMP-2 may relate directly to profound neurodegeneration in AD being a consequence of $A\beta_{42}$-dependent signaling (Zhang et al., 2016). These data may suggest that there are two signaling events triggered by Aβ: one that enhances its phosphorylation through kinase activity; and the other that initiates protease degradation. Whether these independent events can limit bona fide axonal transport of critical molecular cargo for neuronal integrity remains to be elucidated.

It has been demonstrated that the motor protein, kinesin-1, transports molecular cargo proteins into the synapse (Ferreira et al., 1992) and thus is important in axonogenesis (Baas, 1997; Terada et al., 2000). It has also been shown that CRMP-2 can directly interact with kinesin light chain (KLC)

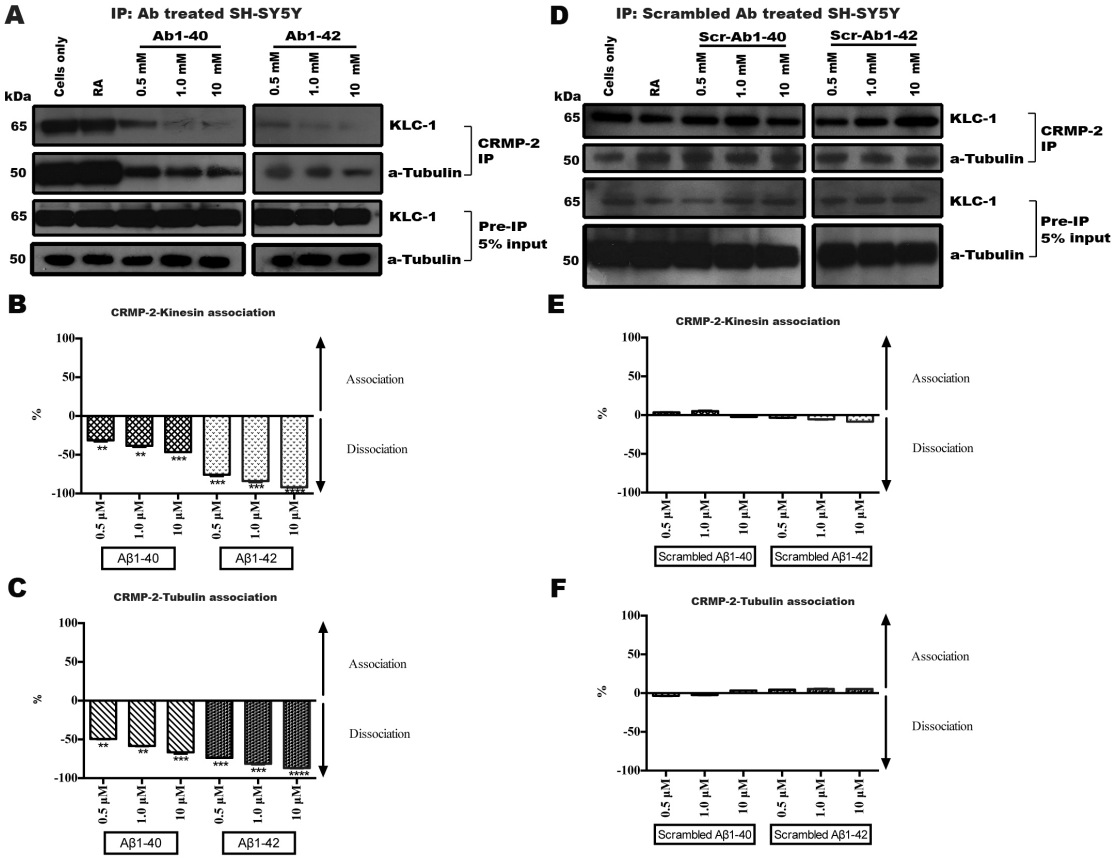

Figure 6 Decreased association of kinesin and tubulin to CRMP-2 in Aβ-treated SH-SY5Y human neuroblastoma cells.
(A) The levels of total kinesin and α-tubulin before and after immunoprecipitation of CRMP-2 from $A\beta_{1–40}$ and $A\beta_{1–42}$-treated SH-SY5Y cells. (B) $A\beta_{1–40}$-treated SH-SY5Ycells had an approximate 50% reduction in CRMP-2 bound kinesin when compared to untreated or cells treated with scrambled $A\beta_{1–40}$ peptide (**P < 0.01; ***P < 0.001). $A\beta_{1–42}$-treated SH-SY5Y cells exhibited an approximate 90% reduction in kinesin association with CRMP-2 when compared with untreated control or cells treated with scrambled $A\beta_{1–42}$ peptide (****P < 0.0001, ***P < 0.001). (C) $A\beta_{1–40}$-treated SH-SY5Y cells show an approximate 60% reduction in α-tubulin associated with CRMP-2 when compared to untreated control or cells treated with scrambled $A\beta_{1–40}$ peptide (***P < 0.001, **P < 0.01). $A\beta_{1–42}$-treated SH-SY5Ycells had an approximate 80% reduction in α-tubulin bound to CRMP-2 when compared with untreated control or cells treated with scrambled $A\beta_{1–42}$ peptide (****P < 0.0001, ***P < 0.001) (n = 3). (D–F) The levels of total kinesin and α-tubulin before and after immunoprecipitation of CRMP-2 from $scrA\beta_{1–40}$ and $scrA\beta_{1–42}$-treated SH-SY5Y cells demonstrate no modulation from basal (untreated) levels. Statistically significant differences were demonstrated following multiple pair-wise comparisons (one-way analysis of variance with Tukey's *post hoc* tests performed). CRMP-2: Collapsin response mediator protein-2.

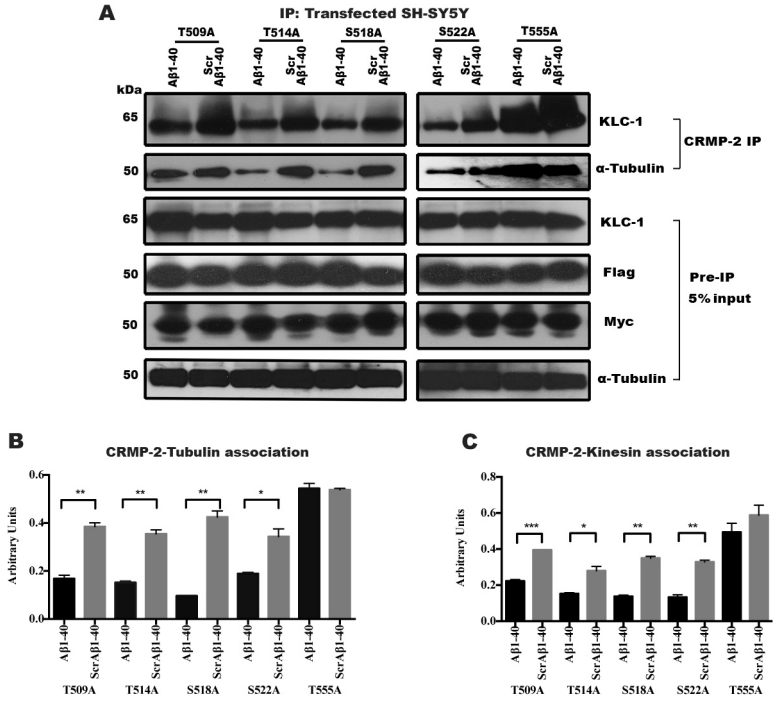

Figure 7 Overexpression of the T555A CRMP2 mutant protein in SH-SY5Y neuroblastoma cells enhances the association of collapsin response mediator protein-2 (CRMP-2) with kinesin and tubulin even in the presence of extracellular Aβ.
(A) Protein lysates from SH-SY5Y cells that were transfected with the CRMP-2 phospho-specific mutant constructs and treated with 10 μM of $A\beta_{1–40}$ or $scrA\beta_{1–40}$ for 24 hours in culture. Anti-Flag and –Myc immunoreactivity illustrate successfully transfection of SH-SY5Y cells. (B) Increased levels of CRMP-2-bound tubulin are also evident in T555A transfected SH-SY5Y cells. Cells transfected with all other constructs show a decrease in tubulin association with CRMP-2 (*P < 0.05, **P < 0.01). (C) Increased levels of CRMP-2-bound kinesin in T555A transfected SH-SY5Y cells are clearly evident even in the presence of increasing concentrations of extracellular Aβ. Cells transfected with the other mutant CRMP-2 constructs show a reduction in the kinesin association (*P < 0.05, **P < 0.01, ***P < 0.001). Statistically significant differences were demonstrated following multiple two-tailed Student's t-tests based on a normal distribution of the data.

(Kimura et al., 2005) and thus link KLC to the proteins that are required to be transported to the growth cone thereby facilitating axon elongation (Fukata et al., 2002; Nishimura et al., 2003; Kimura et al., 2005). Hence, CRMP-2 functions as a cargo receptor for kinesin-1 and carries its interacting molecules such as tubulin heterodimers to the growth cone of the developing axon. This transport system is critical for the organization of the actin cytoskeleton and microtubule assembly in the distal end of the growing axon, thus enhancing axonal outgrowth (Kawano et al., 2005a). In the present study, we found that the interaction of CRMP-2 with kinesin-1 decreases with the increase in $A\beta_{1-40}$ concentration in SH-SY5Y cells. Since this interaction paralleled the increase in CRMP-2 dissociation from tubulin, we hypothesized that the phosphorylation of CRMP-2 was regulating the dissociation of the key motor proteins and molecular cargo. We, therefore, over-expressed different phospho-mutant constructs to abrogate the dissociation effects of phosphorylation of CRMP-2, driven by the increased concentration of extracellular Aβ. We found that, by far the most effective phospho-mutant in abrogating Aβ-dependent kinesin-tubulin dissociation was the T555ACRMP2 mutant, previously utilized by our group to maintain axonal integrity in the mouse model of multiple sclerosis, experimental autoimmune encephalomyelitis (Petratos et al., 2012). However, whether $A\beta_{1-40}$-dependent phosphorylation of CRMP-2 abrogates anterograde axonal transport, and thus axonal outgrowth, remains to be elucidated.

Conclusion

Our data indicate that the phosphorylation of CRMP-2 can elicit neurite dysfunction, initiated through Aβ-signaling. The limitation of this study was that we did not show an abrogation of CRMP-2 phosphorylation-dependent cognitive and neurodegenerative outcomes by genetic means in transgenic AD mice, although these experiments are underway. Current therapeutics in AD target mechanisms to reduce the Aβ load in the brain thereby limiting the cognitive decline and neurodegenerative changes associated with AD. Compounds that can interfere with this adverse Aβ-dependent signaling pathway in AD are of potential therapeutic value as they may limit neurite dystrophy and axonal transport dysfunction, thereby limiting cognitive decline. In this light, our findings suggesting a central role for Aβ-mediated phosphorylation of CRMP-2 leading to neurite dystrophy reveal a potential therapeutic target for AD.

Acknowledgments: *The authors wish to acknowledge the contributions of Monash Micro Imaging (MMI) facilitating microscopy assistance, in particular Stephen Firth, Dr. Judy Callaghan and Dr. Alex Fulcher. Finally, the authors extend their gratitude to the Victorian Brain Bank Network (Project ID# 13.20) for the provision of frozen postmortem brain tissue.*

Author contributions: *SHM conducted most laboratory experiments and wrote the manuscript. MJK grew SH-SY5Y cells, generated, preformed western blotting analysis constructs, and proofread the manuscript. PMA carried out the plaque assay, grew SH-SY5Y cells, generated constructs, and proof-read the manuscript. ST performed immunohistochemical analysis. MMB conducted western blotting. AAA preformed western blotting analysis. JYL and MJK grew SH-SY5Y cells, generated, preformed western blotting analysis of constructs, and proofread the manuscript. DLS performed the mass spectrometry analysis. RK developed CRMP-2 mutant constructs. CM performed autopsies and neuropathological assessment of all human brain tissue. MFA performed the anti-pThr555CRMP-2 antibody validation, proof-read, and edited the manuscript. AB performed transfection and validated the anti-pThr555CRMP-2 antibody. EL conducted the AFM imaging and generated the Figure 4B. PH provided the protocol and conducted the AFM imaging and proofread the manuscript. BW provided the the AFM imaging equipment and protocol. SP conceived and designed the study, performed plaque assays, wrote and edited the manuscript. All authors approved the final version of this manuscript for publication.*

Conflicts of interest: *The authors declare that they have no conflicts of interest.*

Financial support: *SHM was supported by King Abdul-Aziz University postgraduate scholarship. SP was supported by National Multiple Sclerosis Society (USA) Project Grant ID #RG43981/1. None of the funding bodies play any role in the study other than to provide funding.*

Institutional review board statement: *Monash University Human Ethics committee approval number CF13/1646-2013000831 for all human tissue and University of Melbourne Animal Ethics Committee (AEC#06224) for all animal tissue experiments.*

Copyright license agreement: *The Copyright License Agreement has been signed by all authors before publication.*

Data sharing statement: *Datasets analyzed during the current study are available from the corresponding author on reasonable request.*

Plagiarism check: *Checked twice by iThenticate.*

Peer review: *Externally peer reviewed.*

Open access statement: *This is an open access journal, and articles are distributed under the terms of the Creative Commons Attribution-Non-Commercial-ShareAlike 4.0 License, which allows others to remix, tweak, and build upon the work non-commercially, as long as appropriate credit is given and the new creations are licensed under the identical terms.*

Open peer reviewer: *George D. Vavougios, Athens Naval Hospital, Greece.*

Additional files:

Additional Figure 1: *Characterization of anti-Phospho-Thr555 CRMP-2 antibody.*

Additional Table 1: *List of identified proteins.*

References

Arimura N, Menager C, Kawano Y, Yoshimura T, Kawabata S, Hattori A, Fukata Y, Amano M, Goshima Y, Inagaki M, Morone N, Usukura J, Kaibuchi K (2005) Phosphorylation by Rho kinase regulates CRMP-2 activity in growth cones. Mol Cell Biol 25:9973-9984.

Baas PW (1997) Microtubules and axonal growth. Curr Opin Cell Biol 9:29-36.

Bressloff PC, Levien E (2015) Synaptic democracy and vesicular transport in axons. Phys Rev Lett 114:168101.

Bretin S, Reibel S, Charrier E, Maus-Moatti M, Auvergnon N, Thevenoux A, Glowinski J, Rogemond V, Premont J, Honnorat J, Gauchy C (2005) Differential expression of CRMP1, CRMP2A, CRMP2B, and CRMP5 in axons or dendrites of distinct neurons in the mouse brain. J Comp Neurol 486:1-17.

Brown M, Jacobs T, Eickholt B, Ferrari G, Teo M, Monfries C, Qi RZ, Leung T, Lim L, Hall C (2004) Alpha2-chimaerin, cyclin-dependent Kinase 5/p35, and its target collapsin response mediator protein-2 are essential components in semaphorin 3A-induced growth-cone collapse. J Neurosci 24:8994-9004.

Charrier E, Reibel S, Rogemond V, Aguera M, Thomasset N, Honnorat J (2003) Collapsin response mediator proteins (CRMPs): involvement in nervous system development and adult neurodegenerative disorders. Mol Neurobiol 28:51-64.

Fassas A, Passweg JR, Anagnostopoulos A, Kazis A, Kozak T, Havrdova E,Carreras E, Graus F, Kashyap A, Openshaw H, Schipperus M, Deconinck E, Mancardi G, Marmont A, Hansz J, Rabusin M, Zuazu Nagore FJ, Besalduch J, Dentamaro T, Fouillard L, et al. (2002) Hematopoietic stem cell transplantation for multiple sclerosis. A retrospective multicenter study. J Neurol 249:1088-1097.

Ferreira A, Niclas J, Vale RD, Banker G, Kosik KS (1992) Suppression of kinesin expression in cultured hippocampal neurons using antisense oligonucleotides. J Cell Biol 117:595-606.

Fukata Y, Itoh TJ, Kimura T, Menager C, Nishimura T, Shiromizu T, Watanabe H, Inagaki N, Iwamatsu A, Hotani H, Kaibuchi K (2002) CRMP-2 binds to tubulin heterodimers to promote microtubule assembly. Nat Cell Biol 4:583-591.

Goshima Y, Nakamura F, Strittmatter P, Strittmatter SM (1995) Collapsin-induced growth cone collapse mediated by an intracellular protein related to UNC-33. Nature 376:509-514.

Gustke N, Steiner B, Mandelkow EM, Biernat J, Meyer HE, Goedert M, Mandelkow E (1992) The Alzheimer-like phosphorylation of tau protein reduces microtubule binding and involves Ser-Pro and Thr-Pro motifs. FEBS Lett 307:199-205.

Hensley K, Kursula P (2016) Collapsin response mediator protein-2 (CRMP2) is a plausible etiological factor and potential therapeutic target in Alzheimer's disease: comparison and contrast with microtubule-associated protein tau. J Alzheimers Dis 53:1-14.

Hirokawa N, Takemura R (2005) Molecular motors and mechanisms of directional transport in neurons. Nat Rev Neurosci 6:201-214.

Inagaki N, Chihara K, Arimura N, Ménager C, Kawano Y, Matsuo N, Nishimura T, Amano M, Kaibuchi K (2001) CRMP-2 induces axons in cultured hippocampal neurons. Nat Neurosci 4:781-782.

Jin M, Shepardson N, Yang T, Chen G, Walsh D, Selkoe DJ (2011) Soluble amyloid beta-protein dimers isolated from Alzheimer cortex directly induce Tau hyperphosphorylation and neuritic degeneration. Proc Natl Acad Sci U S A 108:5819-5824.

Kawano Y, Yoshimura T, Tsuboi D, Kawabata S, Kaneko-Kawano T, Shirataki H, Takenawa T, Kaibuchi K (2005a) CRMP-2 is involved in kinesin-1-dependent transport of the Sra-1/WAVE1 complex and axon formation. Mol Cell Biol 25:9920-9935.

Kawano Y, Yoshimura T, Tsuboi D, Kawabata S, Kaneko-Kawano T, Shirataki H, Takenawa T, Kaibuchi K (2005b) CRMP-2 is involved in kinesin-1-dependent transport of the Sra-1/WAVE1 complex and axon formation. Mol Cell Biol 25:9920-9935.

Kimura T, Watanabe H, Iwamatsu A, Kaibuchi K (2005) Tubulin and CRMP-2 complex is transported via Kinesin-1. J Neurochem 93:1371-1382.

Lazarov O, Lee M, Peterson DA, Sisodia SS (2002) Evidence that synaptically released β-amyloid accumulates as extracellular deposits in the hippocampus of transgenic mice. J Neurosci 22:9785-9793.

Nishimura T, Fukata Y, Kato K, Yamaguchi T, Matsuura Y, Kamiguchi H, Kaibuchi K (2003) CRMP-2 regulates polarized Numb-mediated endocytosis for axon growth. Nat Cell Biol 5:819-826.

Oriola D, Roth S, Dogterom M, Casademunt J (2015) Formation of helical membrane tubes around microtubules by single-headed kinesin KIF1A. Nat Comm 6:8025.

Petratos S, Li QX, George AJ, Hou X, Kerr ML, Unabia SE, Hatzinisiriou I, Maksel D, Aguilar MI, Small DH (2008) The beta-amyloid protein of Alzheimer's disease increases neuronal CRMP-2 phosphorylation by a Rho-GTP mechanism. Brain 131:90-108.

Petratos S, Ozturk E, Azari MF, Kenny R, Lee JY, Magee KA, Harvey AR, McDonald C, Taghian K, Moussa L, Mun Aui P, Siatskas C, Litwak S, Fehlings MG, Strittmatter SM, Bernard CC (2012) Limiting multiple sclerosis related axonopathy by blocking Nogo receptor and CRMP-2 phosphorylation. Brain 135:1794-1818.

Sherman MA, LaCroix M, Amar F, Larson ME, Forster C, Aguzzi A, Bennett DA, Ramsden M, Lesne SE (2016) Soluble conformers of Abeta and tau alter selective proteins governing axonal transport. J Neurosci 36:9647-9658.

Shinkai-Ouchi F, Yamakawa Y, Hara H, Tobiume M, Nishijima M, Hanada K, Hagiwara K (2010) Identification and structural analysis of C-terminally truncated collapsin response mediator protein-2 in a murine model of prion diseases. Proteome Sci 8:53.

Szpankowski L, Encalada SE, Goldstein LSB (2012) Subpixel colocalization reveals amyloid precursor protein-dependent kinesin-1 and dynein association with axonal vesicles. Proc Natl Acad Sci U S A 109:8582-8587.

Taghian K, Lee JY, Petratos S (2012) Phosphorylation and cleavage of the family of collapsin response mediator proteins may play a central role in neurodegeneration after CNS trauma. J Neurotrauma 29:1728-1735.

Takata K, Kitamura Y, Nakata Y, Matsuoka Y, Tomimoto H, Taniguchi T, Shimohama S (2009) Involvement of WAVE accumulation in Abeta/APP pathology-dependent tangle modification in Alzheimer's disease. Am J Pathol 175:17-24.

Terada S, Kinjo M, Hirokawa N (2000) Oligomeric tubulin in large transporting complex is transported via kinesin in squid giant axons. Cell 103:141-155.

Touma E, Kato S, Fukui K, Koike T (2007) Calpain-mediated cleavage of collapsin response mediator protein (CRMP)-2 during neurite degeneration in mice. Eur J Neurosci 26:3368-3381.

Uchida Y, Ohshima T, Sasaki Y, Suzuki H, Yanai S, Yamashita N, Nakamura F, Takei K, Ihara Y, Mikoshiba K, Kolattukudy P, Honnorat J, Goshima Y (2005) Semaphorin3A signalling is mediated via sequential Cdk5 and GSK3beta phosphorylation of CRMP2: implication of common phosphorylating mechanism underlying axon guidance and Alzheimer's disease. Genes Cells 10:165-179.

Um JW, Nygaard HB, Heiss JK, Kostylev MA, Stagi M, Vortmeyer A, Wisniewski T, Gunther EC, Strittmatter SM (2012) Alzheimer amyloid-beta oligomer bound to postsynaptic prion protein activates Fyn to impair neurons. Nat Neurosci 15:1227-1235.

Veyrac A, Giannetti N, Charrier E, Reymond-Marron I, Aguera M, Rogemond V, Honnorat J, Jourdan F (2005) Expression of collapsin response mediator proteins 1, 2 and 5 is differentially regulated in newly generated and mature neurons of the adult olfactory system. Eur J Neurosci 21:2635-2648.

Vossel KA, Zhang K, Brodbeck J, Daub AC, Sharma P, Finkbeiner S, Cui B, Mucke L (2010) Tau reduction prevents Abeta-induced defects in axonal transport. Science 330:198.

Vossel KA, Xu JC, Fomenko V, Miyamoto T, Suberbielle E, Knox JA, Ho K, Kim DH, Yu GQ, Mucke L (2015) Tau reduction prevents Abeta-induced axonal transport deficits by blocking activation of GSK3beta. J Cell Biol 209:419-433.

Wang LH, Strittmatter SM (1996) A family of rat CRMP genes is differentially expressed in the nervous system. J Neurosci 16:6197-6207.

Westerman MA, Cooper-Blacketer D, Mariash A, Kotilinek L, Kawarabayashi T, Younkin LH, Carlson GA, Younkin SG, Ashe KH (2002) The relationship between Aβ and memory in the Tg2576 mouse model of Alzheimer's disease. J Neurosci 22:1858-1867.

Xing H, Lim YA, Chong JR, Lee JH, Aarsland D, Ballard CG, Francis PT, Chen CP, Lai MK (2016) Increased phosphorylation of collapsin response mediator protein-2 at Thr514 correlates with beta-amyloid burden and synaptic deficits in Lewy body dementias. Mol Brain 9:84.

Yoshimura T, Kawano Y, Arimura N, Kawabata S, Kikuchi A, Kaibuchi K (2005) GSK-3beta regulates phosphorylation of CRMP-2 and neuronal polarity. Cell 120:137-149.

Zempel H, Thies E, Mandelkow E, Mandelkow EM (2010) Abeta oligomers cause localized Ca(2+) elevation, missorting of endogenous Tau into dendrites, Tau phosphorylation, and destruction of microtubules and spines. J Neurosci 30:11938-11950.

Zhang JN, Michel U, Lenz C, Friedel CC, Koster S, d'Hedouville Z, Tonges L, Urlaub H, Bahr M, Lingor P, Koch JC (2016) Calpain-mediated cleavage of collapsin response mediator protein-2 drives acute axonal degeneration. Sci Rep 6:37050.

Zhang Z, Ottens AK, Sadasivan S, Kobeissy FH, Fang T, Hayes RL, Wang KK (2007) Calpain-mediated collapsin response mediator protein-1, -2, and -4 proteolysis after neurotoxic and traumatic brain injury. J Neurotrauma 24:460-472.

(*Copyedited by Li CH, Song LP, Zhao M)*

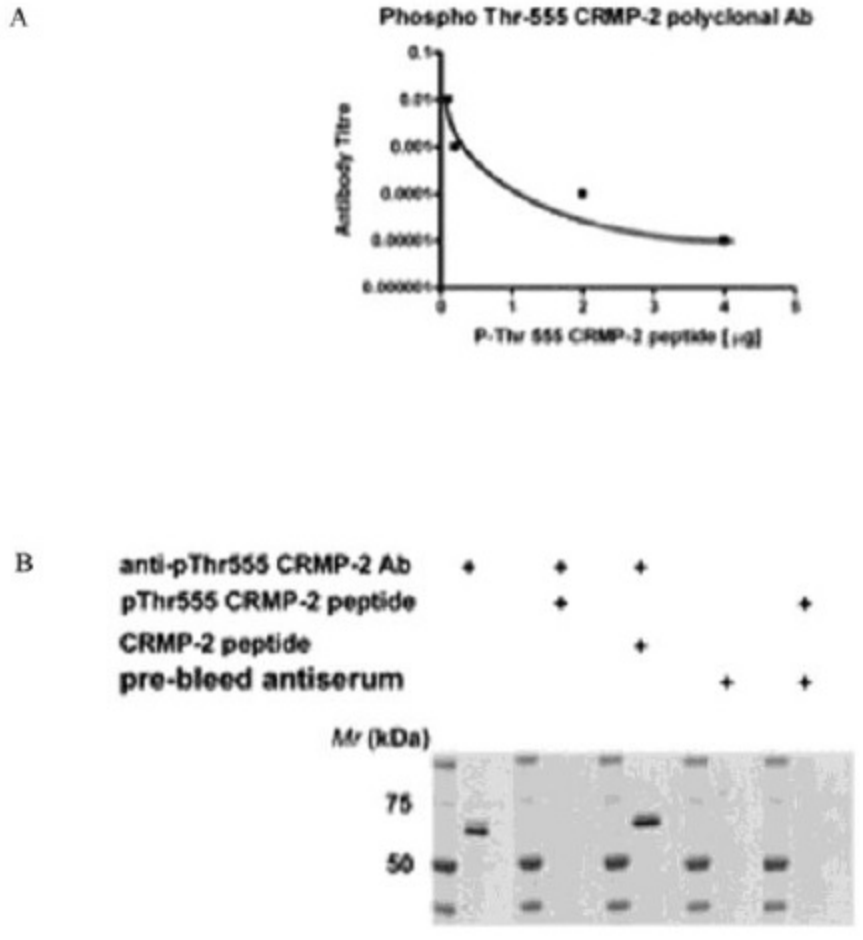

Additional Figure 1 Characterization of anti-Phospho-Thr555 CRMP-2 antibody.

ELISA determining phospho-Thr555 CRMP-2 peptide reactivity with the affinity purified polyclonal antibody (A). Immunoreactivity occurs at 1:10,000 dilution of the anti-Phospho-CRMP-2 antibody with the phospho-CRMP-2 peptide. Tg2576 brain lysates react with the anti-phospho-CRMP-2 antibody by western blot (B). A ~62 kDa band appears with incubation of anti-phospho-CRMP-2 antibody alone and this immunoreactivity can be blocked by pre-incubation of the antibody with the phosphor-Thr555 CRMP-2 peptide. Pre-incubation with the same CRMP-2 peptide without phosphorylation produces the same 62 kDa band. Incubation with the pre-bleed antiserum shows no reactivity with the 62 kDa band (B). The 62 kDa band was then analysed by mass spectrometry and confirmed as phosphorylated CRMP-2.

Additional Table 1 List of identified proteins

Protein	Accession number	Sample	kDa	Mascot search score	Sequence coverage (%)	Total peptides matched
Full length Dihydropyrimidinase-related protein 2 (DPYL2)	Q16555	MS	62.25	17795.06	70.98	59
		MS	62.25	16469.89	70.98	50
		AD	62.25	16849.30	70.98	51
		AD	62.25	15401.93	66.43	53
		FTD	62.25	16776.89	72.90	56
		FTD	62.25	16367.66	63.29	52
		HD	62.25	15660.39	72.90	54
		HD	62.25	14264.21	71.15	51
Cleaved Dihydropyrimidinase-related protein 2 (DPYL2)	Q16555	MS	55	23334.85	67.48	73
		MS	55	29051.38	69.93	91
		AD	55	23831.45	71.85	80
		AD	55	20261.51	69.41	70
		FTD	55	28033.55	71.85	97
		FTD	55	28776.62	71.85	99
		HD	55	21376.15	71.85	72
		HD	55	21669.26	64.16	71
Cleaved Dihydropyrimidinase-related protein 2 (DPYL2)	Q16555	MS	50	7235.23	53.32	23
		AD	50	7097.30	52.45	22
		AD	50	6539.01	38.11	20
		FTD	50	7860.72	48.08	25
		FTD	50	6291.98	43.18	21
		HD	50	13104.91	61.71	44
		HD	50	9667.17	50.87	31